ELSEVIER

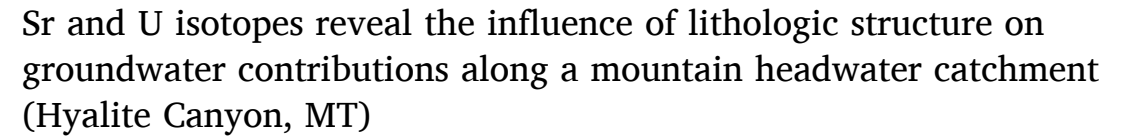
Contents lists available at ScienceDirect

## Journal of Hydrology

journal homepage: www.elsevier.com/locate/jhydrol



### Research papers



Florence R. Miller <sup>a</sup>, Stephanie A. Ewing <sup>a,\*</sup>, Robert A. Payn <sup>a,b</sup>, James B. Paces <sup>c</sup>, Sam J. Leuthold <sup>a,d</sup>, Stephan G. Custer <sup>e</sup>

- <sup>a</sup> Department of Land Resources & Environmental Sciences, Montana State University, United States
- <sup>b</sup> Montana Institute on Ecosystems, United States
- <sup>c</sup> U.S. Geologic Survey, Denver, CO, United States
- <sup>d</sup> Integrated Plant and Soil Sciences Department, University of Kentucky, United States
- <sup>e</sup> Department of Earth Sciences, Montana State University (emeritus), United States

### ARTICLE INFO

This manuscript was handled by Huaming Guo, Editor-in-Chief, with the assistance of Philippe Negrel, Associate Editor

Keywords: Mountain catchment Groundwater Uranium Strontium Geochemical tracer

#### ABSTRACT

Changing precipitation patterns are projected to reduce snowpack storage and late summer stream flows in mountain headwaters of the western United States. Ecosystems, agriculture, and municipalities depend on late summer flow in streams supplying water to the mountain front. Therefore, improved understanding of groundwater storage contributions to mountain streams is increasingly important. In this work, we use <sup>87</sup>Sr/<sup>86</sup>Sr ratios and <sup>234</sup>U/<sup>238</sup>U activity ratios ([<sup>234</sup>U/<sup>238</sup>U]) as indicators of water-rock interaction contributing to runoff, groundwater, and surface-subsurface hydrologic exchanges along Hyalite Creek, a mountain headwater tributary within the upper Missouri River basin. Main stem and tributary flow was sampled longitudinally from 2016 to 2018, focusing on presumed baseflow conditions in February and August. Changing stream chemistry of the main stem is associated with groundwater inflows from local springs discharging from Madison Group limestones, and inputs of water from the Archean gneiss exposed along the mountain front. We use mixing models to estimate that locally in the stream reach traversing a spring outlet, distinct inflows from the Madison aquifer contribute ~4% of streamflow during baseflow conditions. Contributions to streamflow by local inflows from Archean gneiss varied seasonally, with increases in  $^{87}$ Sr/ $^{86}$ Sr values in Hyalite Creek that suggest contributions of  $\sim$ 2% in August to  $\sim$ 8% in February; at the same time, decreasing [ $^{234}\text{U}/^{238}\text{U}$ ] values indicate an otherwise undetected additional endmember, and <sup>222</sup>Rn assays show that total inflows are likely more extensive. Our results reveal distinct groundwater contributions to streamflow from specific rock units within this mountain headwater system, and elucidate pathways of mountain stream flow generation in lithologically diverse watersheds.

#### 1. Introduction

Mountainous regions of the western United States face impending water management challenges, given the combination of urban growth and water scarcity driven by projected changes in precipitation and snowpack dynamics (Knowles et al., 2005; Silverman et al., 2013). The region supports both urban and rural communities that rely heavily on mountain headwaters for municipal and agricultural water supplies (Silverman and Maneta, 2016; Hoylman et al., 2018). These headwater catchments supply a majority of the water found in the rivers and aquifers of intermountain basins (Wilson and Guan, 2004), where more

intensive human land and water use tends to occur. However, the nature and extent of groundwater storage influence on these mountain headwater contributions is generally poorly quantified, leading to uncertainty in estimates of mountain headwater contributions to water-resource availability during low-flow conditions. This study uses geochemical tracers to explore the longitudinal and temporal distribution of groundwater contributions to baseflow conditions in a mountain headwater stream, focusing on a canyon within the upper Missouri and Gallatin River Watersheds (Fig. 1). We demonstrate that chemical and isotopic analyses of weathering products found in stream solute loads provide a useful tool for inferring groundwater contributions from

E-mail address: stephanie.ewing@montana.edu (S.A. Ewing).



<sup>\*</sup> Corresponding author.

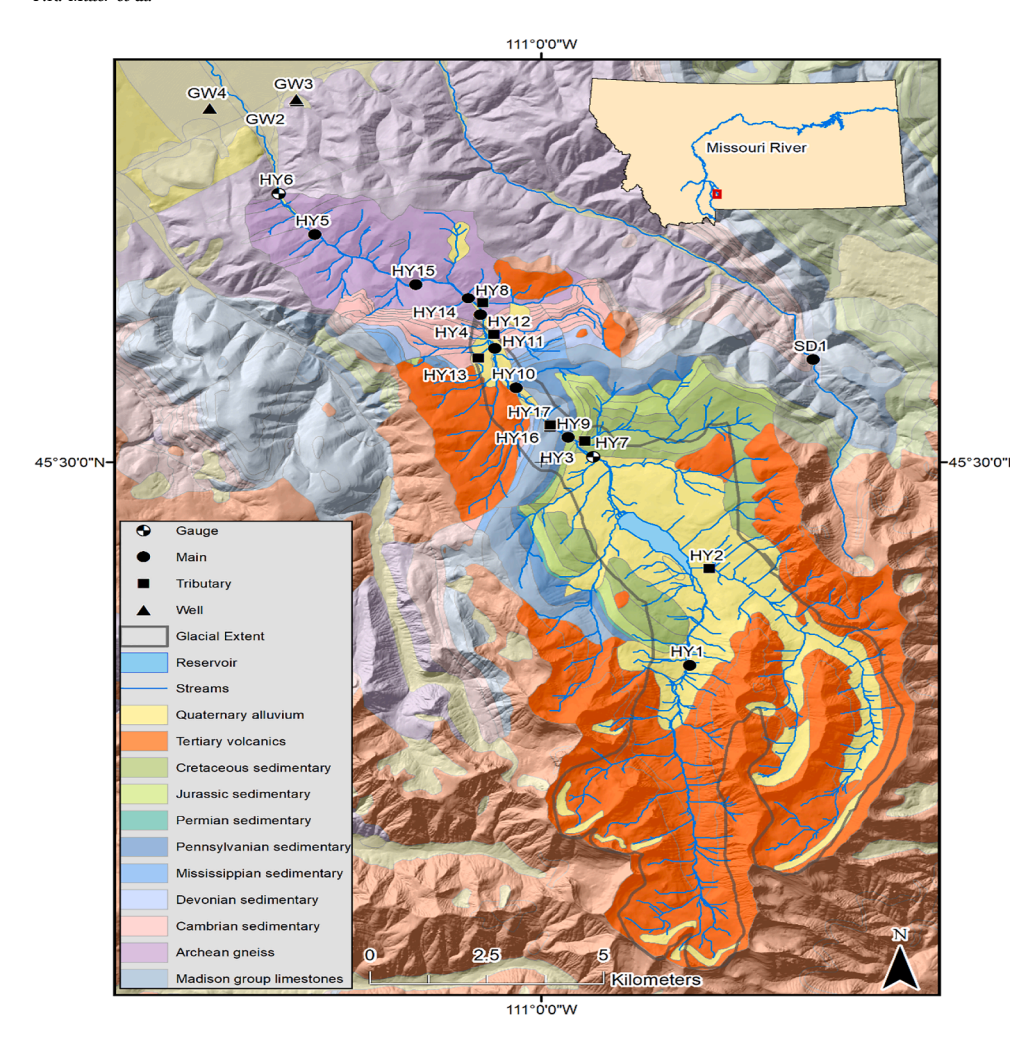


Fig. 1. Geologic map of study area showing sample sites and gauge locations in Hyalite Canvon, Locations are numbered as specified in Table 1 for sites in Hyalite Creek and its tributaries (HY1-HY17) and wells at the canyon outlet (GW4), in Hodgman Canyon (GW2, GW3), and in Sourdough Canyon (SD1). Glacial extent represents extrapolation of moraines thought to reflect Pinedale ( $\sim$ 30 to 15 ka) and Bull Lake ( $\sim$ 180 to 130 ka) glaciations per Weber (1965). Major lithologic units include the Eocene age Absaroka volcanics (red) and associated tills (vellow) at highest elevations, Cretaceous to Cambrian age sedimentary units (greens and blues) at intermediate elevations, and Archean age gneiss along the mountain front (purple) at lowest elevations. The Hyalite Creek watershed is shown in brighter colors. The inset of the state of Montana shows the study area in red, with the Missouri River and its three tributaries in blue (from west to east: Jefferson, Madison, and Gallatin Rivers).

different parts of the watershed. This case study of a mountain headwaters process domain (Montgomery, 1999) holds general insight for understanding the contribution of mountain headwater groundwater storage to intermountain basin communities and ecosystems, and its likely relevance under low-flow conditions and over time.

Mountain headwaters are often characterized by steep mountain streams with fundamental control of geomorphologic development by lithology, structural features, tectonic regime, fluvial erosion or deposition, and glaciation (Amundson et al., 2015; Dixon et al., 2016). Weathering in higher elevation mountain headwater process domains is generally limited by relatively low temperatures and rapid mechanical erosion, compared to lower elevation intermountain basin process domains. As a result, soils in mountain headwater catchments are generally thin and less developed in terms of mineral transformation and mass loss to chemical weathering. Furthermore, high relief results in strong influence of hillslope aspect on the extent of substrate weathering (Hinckley et al., 2014), and topography strongly influences seasonal precipitation and runoff (McGuire et al., 2005; Jencso et al., 2009; Jencso and McGlynn, 2011; Emanuel et al., 2014). Along a mountain headwater valley, stream water solutes reflect the exchanges between surface water and groundwater throughout the mountain headwaters (Payn et al., 2009). These concomitant gains and losses of water along a stream result in longitudinal patterns of solute composition, reflecting dilution and solute-load inputs characteristic of transport of weathering products (or lack thereof) to the stream (Covino and McGlynn, 2007; Capell et al., 2011; Jasechko, 2016; Jasechko and Kirchner, 2016; Yang et al., 2017). Thus, mountain headwaters are key in controlling both streamflow and water quality. Water emerging at the mountain front provides a fingerprint of lithologies within the mountain catchment delivering it, and patterns in water quality along the stream provide information about the spatial distribution of groundwater sources contributing to stream flow generation.

Most work in mountain headwater watersheds has been focused on topographic controls on event flow contributions to streamflow (McGlynn and McDonnell, 2003; McGuire et al., 2005; Jencso and McGlynn, 2011). The study of baseflow generation in mountain headwaters has received less attention, particularly in snowmelt-dominated systems (Soulsby and Tetzlaff, 2008; Payn et al., 2012). However, changes in climate and the distribution of precipitation demand a better understanding of the mechanisms controlling variation in groundwater contributions to baseflow, particularly in semi-arid systems where water-resource availability during dry seasons is a major concern (Soulsby and Tetzlaff, 2008). A first step to understanding the longer-term storage that serves as a reservoir for baseflow is to identify the location and relative contribution from aquifers that contribute to lower stream flows across a catchment.

Geochemical tracers of baseflow sourced by aquifers of varying size, materials, and residence times offer an opportunity to investigate a distinctive signal of groundwater contribution to streamflow. Often these tracers record a signal of both weathering and aquifer flowpath or transit time (Chabaux et al., 2003; Hogan and Blum, 2003; Dosseto et al., 2014). Therefore, the geochemical signal imparted on groundwater contributing to baseflow varies with the chemical composition, age, and weathering susceptibility of the aquifer rock or geomorphic units. As lithology changes throughout the reach of a mountain stream and across the mountain front, so does the cumulative geochemical fingerprint

imparted on the water. These fingerprints can allow baseflow at the outlet to be traced back to its host rock or sediment and allow longitudinal surveys of water quality at baseflow to reveal the location and relative contribution of discharge from specific aquifers to the stream. This study uses  $^{87}{\rm Sr}/^{86}{\rm Sr}$  and  $[^{234}{\rm U}/^{238}{\rm U}]$  values (square brackets denote activity ratio) as natural geochemical tracers to investigate the sources and pathways of water contributing to streamflow during baseflow conditions.

Over the past two decades, many studies have used Sr isotope ratios (primarily  $^{87}$ Sr/ $^{86}$ Sr, but also  $^{88}$ Sr/ $^{86}$ Sr) to examine weathering sequences, dust inputs, and carbonate accumulation in rocks and soils (Bullen et al., 1997; Capo et al., 1998; Capo and Chadwick, 1999; Hart et al., 2004; Chadwick et al., 2009; White et al., 2009). In surface water and groundwater systems, <sup>87</sup>Sr/<sup>86</sup>Sr data have been used to trace sources of soil and rock weathering inputs to stream geochemistry (Horton et al., 1999; Jacobson et al., 2002, 2003; Frost and Toner, 2004). More recently, U-series isotopes, notably [234U/238U], have been used to examine processes of water-rock interaction that rely on the balance between recoil effects that increase [<sup>234</sup>U/<sup>238</sup>U], and bulk U dissolution that decreases [234U/238U] (Bourdon et al., 2003; Chabaux et al., 2003; Dosseto et al., 2008; DePaolo et al., 2006). Water/rock interactions with the different lithologies or flow paths present in the watershed have the potential to result in unique <sup>87</sup>Sr/<sup>86</sup>Sr and [<sup>234</sup>U/<sup>238</sup>U] isotopic signatures, which may allow determination of multiple sources, pathways and mixing relations among end members (Drexler et al., 2014; Paces and Wurster, 2014). Both U and Sr are readily soluble in oxidizing aqueous systems and their radiogenic isotopes are not affected substantially by mass dependent fractionation in near-surface environments (Paces and Wurster, 2014). Thus, Sr- and U-isotopes can potentially provide a precise and accurate fingerprint of water sources and hydrologic evolution (Roback et al., 2001; Faure and Mensing, 2005; Ryu et al., 2009; Pierret et al., 2014; Paces et al., 2015). Together, U and Sr isotopic ratios provide a useful means of examining the influence of weathering processes, water sources, and the degree of water-rock interaction on stream geochemistry, using reactive transport modeling and end member mixing analysis approaches (DePaolo et al., 2006; Maher et al., 2006; Paces and Wurster, 2014).

Here, we explore how aquifer contributions of spatiotemporally variable geochemical weathering products influence baseflow generation in a mountain headwater catchment, using Hyalite Creek in southwestern Montana as a case study. Hyalite Creek is a steep, glaciated, mountain headwater stream with a watershed area of approximately 126 km², draining into the intermountain basin and associated alluvial aquifer of the Gallatin Valley. We use [ $^{234}$ U/ $^{238}$ U] and  $^{87}$ Sr/ $^{86}$ Sr values, along with complementary  $^{222}$ Rn activities, to examine water flow and storage dynamics along the main stem of this mountain stream, with a goal of characterizing a spatially explicit map of the influence of aquifers hosted in four lithologic units with distinct U and Sr isotopic character, and the resulting effects on water quality and supply at the watershed outlet. This work reveals how baseflow and storage dynamics can vary across a catchment that includes lithologic units with variable chemical compositions, ages, and degrees of weatherability.

### 2. Methods

### 2.1. Study area

Hyalite Creek in southwestern Montana traverses a number of bedrock lithologies, providing a case study for assessing cumulative contributions of multiple geochemically diverse aquifers to baseflow along the canyon. The study watershed is located in the north-central Gallatin Mountain Range and is a headwater catchment of the Gallatin River (Fig. 1). Hyalite Creek is dammed midway up Hyalite Canyon, creating a reservoir that supplies one-third of Bozeman's municipal water supply, along with water for irrigated agriculture in the Gallatin Valley (DNRC, 2014). Flow out of Hyalite Creek has been diverted at the

Table 1
Hyalite Creek sample description, elevation, location, and influencing lithology.

Site ID	Location	Elevation (m)	Latitude	Longitude	Influencing Lithology Tertiary Volcanics		
HY1	Hyalite Creek above reservoir	2087	45.452	-110.959			
HY2	Emerald Creek	2063	45.475	-110.954	Tertiary Volcanics		
НҮ7	Hyalite Creek below reservoir at DNRC gauge 41H 2000	1962	45.501	-110.986	Cretaceous Sedimentary		
НҮЗ	Lick Creek	1960	45.505	-110.988	Cretaceous Sedimentary		
HY9	Hyalite Creek below Lick Creek	1941	45.506	-110.993	Jurassic Sedimentary		
HY16	Madison limestone spring channel	1936	45.508	-110.998	Mississippian Sedimentary		
HY17	Madison limestone spring seep	1931	45.509	-110.997	Mississippian Sedimentary		
HY10	Middle Hyalite Creek	1909	45.517	-111.007	Mississippian Sedimentary		
HY11	Hyalite Creek at Langohr Logging Road	1882	45.527	-111.013	Cambrian Sedimentary		
НҮ13	Unnamed creek in terminal glacial moraine meadow	1898	45.524	-111.017	Cambrian Sedimentary		
HY12	Buckskin Creek	1889	45.530	-111.013	Cambrian Sedimentary		
HY4	Hyalite Creek at Langohr's Campground	1861	45.535	-111.017	Cambrian Sedimentary		
HY8	Moser Creek	1871	45.537	-111.016	Cambrian Sedimentary/ Archean Gneiss		
HY14	Hyalite Creek below Moser Creek	1854	45.539	-111.020	Archean Gneiss		
HY15	Hyalite Creek above Practice Rock	1729	45.554	-111.062	Archean Gneiss		
HY5	Hyalite Creek at Practice Rock	1807	45.542	-111.034	Archean Gneiss		
HY6	Hyalite Creek at USGS gauge 06,050,000	1690	45.563	-111.072	Archean Gneiss		
SD1	Sourdough Creek	1926	45.524	-110.926	Archean Gneiss		
GW2	Hodgman Canyon - gneiss spring	1704	45.585	-111.067	Archean Gneiss		
GW3	Hodgman Canyon - gneiss well	1692	45.586	-111.067	Archean Gneiss		
GW4	Hyalite Creek alluvial fan well	1641	45.583	-111.091	Quaternary Alluvium		

mountain front as a water source for irrigation since 1871 (Kramer, 2013). In addition, Hyalite Canyon has an extensive logging history beginning in the 1870s through 1911 (Kramer, 2013). Currently, Hyalite Canyon is heavily used for recreation with about 80,000 visitors per month during the peak summer season (Gedeon, 2015).

Soils in Hyalite Canyon reflect limited chemical weathering and strong influence of parent lithologies (United States Department of Agriculture, 1996). In meadows and open slopes, soils classified as Mollisols have developed with relatively thick, dark A horizons. In forested areas, soils classified as Alfisols and Inceptisols have developed with thin A horizons, occasional E horizons indicating strong leaching, and subsurface horizons with enhanced clay content.

Hyalite Canyon receives an average of 82 cm of precipitation annually (30-year average 1981–2010) (USDA NRCS; Prism Climate Group), with 40% of that falling as snow. At an elevation of 2469 m, the maximum mean monthly temperature is 14  $^{\circ}$ C in July and the minimum monthly mean temperature is -7.7  $^{\circ}$ C in December (Shower Falls Sno-Tel, USDA NRCS). Vegetation in Hyalite Canyon is primarily evergreen coniferous forest, with dominant species of lodgepole pine (*Pinus contorta*), subalpine fir (*Abies lasocarpa*), and Douglas fir (*Pseudotsuga menziesii*).

### 2.2. Sample site selection

Sampling sites (Table 1) were selected to represent potential contributions from rock units with distinct geochemical character (Fig. 1, Table 2). Sampling sites included surface waters in Hyalite Creek and five tributaries (HY1 through HY15), a spring and associated spring channel in the bank of Hyalite Creek (HY16 and HY17), a well and associated cistern in neighboring Hodgman Canyon (GW2 and GW3), and a well in the uppermost alluvial fan formed by Hyalite Creek at the mountain front (GW4) (Fig. 1). Surface waters were sampled in February and August 2016–2018, when baseflow conditions were presumed to dominate stream flow generation based on hydrograph levels.

We started with six primary surface water sites along Hyalite Creek in 2016, targeting delineation of waters influenced by the major lithologic units (HY1 through HY6, labeled sequentially with decreasing elevation). We expanded the number of sites between 2016 and 2018, based on identification of reaches with notable longitudinal changes in chemistry and their potential end member contributors. Ultimately, sample sites included ten main stem locations (in order of decreasing elevation: HY1, HY7, HY9, HY10, HY11, HY4, HY14, HY15, HY5, HY6), five tributaries (HY2, HY3, HY12, HY13, HY8), two springs (HY16,

**Table 2**Selected <sup>87</sup>Sr/<sup>86</sup>Sr values in bedrock units or groundwaters salient to this work.

Unit Description	Sample Type	<sup>87</sup> Sr/ <sup>86</sup> Sr	Reference
Absaroka Volcanic rock units (WY)	Rock	0.70433-0.70826	Feeley & Cosca, 2003; Lindsay & Feeley, 2003
Absaroka Volcanics (MT and WY)	Rock	0.70543	Hiza, 1999
Carbonates (average, Yellowstone National Park)	Rock	0.71062	Kharaka et al., 1991
Madison Limestone Formation (Bighorn Basin, MT)	Rock	0.70883	Moore-Nall, 2016
Madison Paleokarst (Bighorn Basin, WY)	Rock	0.70875	Frost & Toner, 2004
Madison limestone (Bighorn Basin, WY)	Rock	0.70809	Frost & Toner, 2004
Archean age granitics (Beartooth Mountains, MT)	Rock	0.70617-0.78304	Wooden & Mueller, 1988
Catchments draining Eocean Absaroka volcanics (Clark's Fork, WY/MT)	Water	0.704–0.705	Horton et al., 1999
Catchments draining Paleozoic sedimentary units (Clark's Fork, WY/ MT)	Water	0.704–0.708	Horton et al., 1999
Catchments draining Precambrian granitic gneiss units (Clark's Fork, WY/ MT)	Water	0.721-0.732	Horton et al., 1999

HY17), three wells (GW2, GW3, GW4), and one neighboring stream (Sourdough Creek, also known as Bozeman Creek) in the next major valley to the east (SD1) (Table 1, Fig. 1).

Two sampling locations were co-located at sites with continuous stream gauges along Hyalite Creek. Site HY7 is co-located with a Montana Department of Natural Resources and Conservation gauge (DNRC; number 41H 2000) downstream of Hyalite Reservoir, and HY6 is colocated with a U.S. Geological Survey gauge (USGS; number 06050000) located at the mouth of Hyalite Canyon (Table 1, Fig. 1). Hydrographs from these two gauges depict a snowmelt dominated hydrologic regime (Fig. 2), with flows ranging from 0.18 to 5.34 m<sup>3</sup> s<sup>-1</sup> at the DNRC gauge (HY7) and from 0.48 to 7.51 m<sup>3</sup> s<sup>-1</sup> at the USGS gauge (HY6) during the sampling period from 2016 to 2018. Hydrographs show how our sampling events align with lower flow conditions (Fig. 2, note log scale), where August sampling dates reflect low summer flows and February sampling dates reflect low winter flows. On a given sampling date, flow in the main stem of Hyalite Creek increased between the two gauges at sites HY7 and HY6: on 2/19/2016 from 0.34 to 0.55 m<sup>3</sup>  $s^{-1}$  (net gain of 0.21 m<sup>3</sup> s<sup>-1</sup> or a 62% increase), on 8/24/2016 from 1.40 to 1.65  $\rm m^3\,s^{-1}$  (net gain of 0.25  $\rm m^3\,s^{-1}$  or a 18% increase), and on 8/23/ 2017 from 1.14 to 1.57  $\text{m}^3 \text{ s}^{-1}$  (net gain of 0.43  $\text{m}^3 \text{ s}^{-1}$  or a 38% increase). Gauge data were not available for HY7 during the 2/4/2017 sampling due to interference from freezing. Thus, net gains in discharge between HY7 and HY6 were similar in absolute volume between February and August, but those gains represent a proportionally larger fraction of stream flow during February due to lower flow conditions in

Hyalite Creek traverses a range of lithologic units known to have distinct geochemical character (Table 2), from the highest sample site at 3140 m above sea level to the lowest site near the mountain front at an elevation of 1690 m above sea level (Fig. 1) (Berg et al., 1999, 2000; Vuke et al., 2002, 2007; Kellogg and Williams, 2006). Specific contributions of rock weathering products to Hyalite Creek water will depend on differential mineral weatherability; however, the general range of <sup>87</sup>Sr/<sup>86</sup>Sr values observed for these lithologies is substantial enough to use <sup>87</sup>Sr/<sup>86</sup>Sr data to fingerprint water/rock interactions. Uppermost Hyalite Creek (3140-2100 m elevation) is underlain by Eocene-aged andesitic to basaltic rocks of the Washburn Group within the Absaroka Volcanic Supergroup. Sample sites located in the steep glaciated terrain cutting volcanic rocks include Upper Hyalite Creek (HY1) and Emerald Creek tributary (HY2), both located above Hyalite Reservoir (Fig. 1). These Eocene volcanic rocks cap a sequence of Cretaceous- to Cambrianaged sedimentary rocks exposed in the middle elevations of Hyalite Canyon (2010 to 1875 m). Lithologies include a succession of shales, limestones, siltstones, and sandstones that are progressively older with decreasing elevation (Fig. 1). Main stem sites HY7 and HY9 are located at the transition from Eocene volcanic to Cretaceous sedimentary lithologies downstream of Hyalite Reservoir. Lick Creek (HY3) is a tributary that joins the main stem between those two sites and drains Mesozoic siliciclastic sedimentary units including the Cretaceous-aged Thermopolis shale. Mississippian-aged Madison Group limestones are exposed further downstream at elevations of 1925 to 1915 m (Kirk, 2002). At an elevation of 1920 m, a spring (HY16) and associated spring channel (HY17) discharge from the Madison aquifer, an important regional karst aquifer known to contribute flow to springs and baseflow in the neighboring Sourdough Canyon (Kirk, 2002), as well as to baseflow in neighboring Gallatin Canyon and Hyalite Canyon. The main stem of Hyalite Creek crosses Mississippian- to Cambrian-aged sedimentary rock units at elevations of 1910 to 1860 m, and includes sites HY10, HY11, and HY4. Tributaries Buckskin Creek (HY12), 'Meadow' Creek (HY13), and Moser Creek (HY8) drain areas underlain by those same Paleozoic sedimentary rock units, although the Moser Creek subwatershed includes Archean gneisses and both the Moser and 'Meadow' Creek subwatersheds include Eocene volcanics (Fig. 1). At its lowest elevations (1875 to 1690 m), Hyalite Creek cuts a narrow, unglaciated canyon through Archean quartzofeldspathic gneiss. Main stem sites

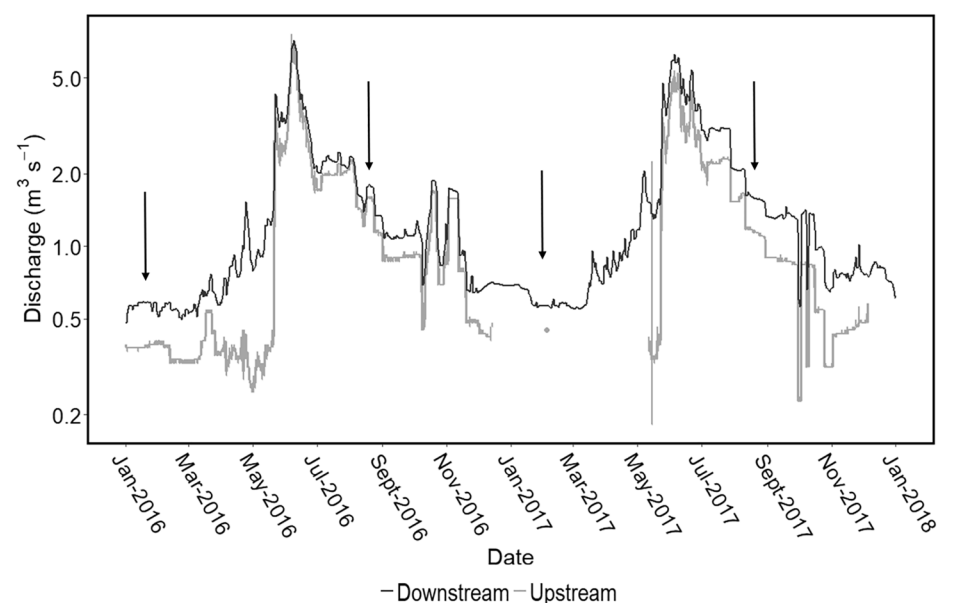


Fig. 2. Hyalite Creek discharge on a logarithmic scale. Measurements from 1/1/2016 to 1/1/2018 at the DNRC stream gauge (site HY7; hourly discharge measurements; light gray) and at the USGS stream gauge (site HY6; daily mean discharge; dark gray). Gray dot indicates measured discharge (area-velocity method) taken during 2/4/2017 sampling at site HY7 while gauge was not recording measurements due to ice. Arrows indicate sample dates targeting baseflow conditions in February (2016–2017) and August (2016–2017). Gauge locations shown on Fig. 1 (U.S. Geological Survey, 2018, Montana DNRC, 2018).

HY14 and HY15 are located near the transition between sedimentary bedrock and gneiss near an elevation of 1875 m. Main stem site HY5 is located at an elevation of 1730 m, and site HY6 is located near the mountain front at an elevation of 1690 m, just downstream of a shear zone within the Archean gneiss (May, 1985). Groundwater present in fractured Archean gneiss was sampled at a spring-fed cistern and nearby well in the neighboring Hodgman Canyon (GW2, GW3) at 1690 m elevation. Groundwater from site GW4, a residential well located in the uppermost part of the Hyalite Creek alluvial fan (Fig. 1), is thought to represent water originating from mountain front recharge of the Gallatin Valley aquifer from Hyalite Creek.

Moraines deposited from the most recent Pinedale glaciation period (~30 to 15 ka) are present within the headwaters of Hyalite and Emerald Creeks (HY1, HY2) and extend downstream nearly to Hyalite Creek's convergence with Lick Creek (HY3) at an elevation of about 1975 m (Weber, 1965). Moraines interpreted as resulting from the Pinedale glaciation indicate erosion of Absaroka volcanic rocks in the upper reaches of Hyalite Creek through Jurassic-aged sedimentary rocks in the middle elevations of the stream (Fig. 1). Moraines interpreted as resulting from the older Bull Lake glaciation (~180 to 130 ka) extend further down canyon, from the headwaters of Hyalite and Emerald Creeks (HY1, HY2) to just above Langohr Campground (HY4) at an elevation of about 1860 m (Weber, 1965). These moraines pass through Devonian to Cambrian-aged sedimentary rock units between elevations of 1975 and 1850 m. The canyon narrows abruptly downstream from the terminus of moraines associated with Bull Lake glaciation, and remains relatively steep and narrow through the Archean gneiss.

### 2.3. Water sampling procedures and solute analysis

Surface water samples were collected using a peristaltic pump (Geotech  $^{\rm TM}$  Denver, CO, United States) with platinum-cured Silicon tubing. Samples were filtered at the time of sampling using a 0.45  $\mu m$ , mid-capacity capsule filter (Geotech  $^{\rm TM}$  Denver, CO, United States). Insitu temperature, pH, specific electrical conductivity (SC), and dissolved oxygen (DO) were measured at each sampling site using a handheld multimeter (YSI 556 Yellow Springs, OH, USA). Alkalinity was measured in the field using colorimetric titration (Hach  $^{\rm TM}$  kit; phenolphthalein/bromethymol blue and  $\rm H_2SO_4$ ). When conditions allowed, discharge was measured using the area-velocity method, where water velocities were measured using an electromagnetic flow meter (Marsh McBirney / Hach  $^{\rm TM}$  Loveland, CO, United States). Comparison of

continuous gauge data with area-velocity measured discharge suggests uncertainty of about 10% among the gauging methods and in any given discharge measurement. Wells were sampled by purging three well volumes prior to water collection, employing the same filtration and field measures used at surface water sampling sites.

Chemical and isotopic analyses were conducted at Montana State University (MSU) in Bozeman, MT, the Montana Bureau of Mines and Geology (MBMG) in Butte, MT, and the USGS Southwest Isotope Research Laboratory (SWIRL) in Denver, CO. Major cations and trace metal concentrations were analyzed by Inductively Coupled Plasma -Optical Emission Spectroscopy (ICP-OES; Perkin Elmer<sup>TM</sup> Waltham, MA, United States) at MBMG and the MSU Environmental Analytical Laboratory, and by inductively coupled plasma mass spectrometry (ICP-MS) at MBMG. Radiogenic isotope ratios  $^{87}$ Sr/ $^{86}$ Sr and  $[^{234}$ U/ $^{238}$ U] as well as U concentrations were measured by thermal ionization mass spectrometry (TIMS) at SWIRL. In March of 2018, to compliment results to date, we conducted a longitudinal survey of <sup>222</sup>Rn concentrations at our established sampling sites (Hoehn et al., 1992; Schubert et al., 2006; Gardner et al., 2011). Samples were collected as described in Gardner et al. (2011) and analyzed at the University of Montana using scintillation counting.

U and Sr isotopic analysis followed procedures described in Ewing et al. (2015) and Paces & Wurster (2014). Water samples, field blanks, procedural blanks, and standards of known composition were prepared for U and Sr isotopic analysis at the MSU Soil Biogeochemistry laboratory. The amount of sample processed was based on U concentrations, which were much lower than Sr concentrations, as expected in natural waters (Table 3). Sample volumes containing ~100 ng U and 0.01 -0.13 mg Sr were weighed in 500 mL Teflon containers, acidified with 1-2 mL of trace metal grade (TMG) concentrated HNO<sub>3</sub>, and spiked with known amounts of highly purified <sup>236</sup>U-spike solution to allow determination of U concentration by isotope dilution. Field and procedural blanks were spiked with known amounts of both <sup>236</sup>U and <sup>84</sup>Sr. Water samples were completely evaporated on a hotplate in an exhausting HEPA-filtered clean hood. The residual solids were dissolved with approximately 5-10 mL of TMG ~7 N HNO<sub>3</sub>, transferred to 15 mL Teflon vials, and were again evaporated. If dissolved organic carbon (DOC) concentrations were > 10 mg L<sup>-1</sup>, re-dissolved samples were transferred to pre-cleaned quartz crucibles, evaporated to dryness, and heated to 550 °C in a muffle furnace for one hour to remove organic compounds. Combusted residues were dissolved in 10–15 mL of  $\sim$ 7 N TMG HNO<sub>3</sub>, transferred to 15 mL Teflon vials and evaporated. Residual solids from

Table 3 Select solute concentrations and isotope values for individual water samples.

Site ID	Description	Sample Date	Ca (mg L <sup>-1</sup> ) MDL*: 0.0060	Sr (mg L <sup>-1</sup> ) MDL*: 0.0066	U (ug L <sup>-1</sup> )	$\pm 2\sigma$	Ca/ Sr	<sup>87</sup> Sr/ <sup>86</sup> Sr	$\pm 2\sigma$	[ <sup>234</sup> U/ <sup>238</sup> U] #	$\pm 2\sigma$	Alk** (mg L <sup>-1</sup> )
HY1	Hyalite Creek above reservoir	2/19/16	3.07	0.02	0.005	0.0001	176	0.708832	0.000009	1.722	0.022	
		8/25/16	3.75	0.02	0.014	0.0001	188	0.708853	0.000010	1.695	0.013	18
		2/4/17	3.79		0.015	0.0002		0.708898	0.000009	1.642	0.012	15
		8/23/17	3.78	0.02	0.005	0.0000	179	0.709214	0.000010	1.616	0.025	
HY2	Emerald Creek	2/19/16	4.60	0.03	0.014	0.0001	172	0.708900	0.000009	1.629	0.006	
		8/25/16	5.67	0.03	0.012	0.0001	186	0.708904	0.000009	1.691	0.012	29
		2/4/17	5.87	0.03	0.012	0.0001	196	0.708900	0.000009	1.645	0.006	24
		8/23/17	5.56	0.03	0.011	0.0001	178	0.708953	0.000009	1.671	0.010	28
HY7	Hyalite Creek below reservoir at DNRC gauge 41H 2000	2/4/17	9.33	0.04	0.242	0.0024	249	0.708712	0.000010	1.591	0.006	35
		8/23/17	7.00	0.03	0.023	0.0002	231	0.708701	0.000009	1.621	0.007	12
HY3	Lick Creek	2/19/16	21.65	0.08	0.536	0.0054	277	0.708458	0.000010	1.570	0.004	
		8/25/16	44.60	0.14	0.203	0.0020	321	0.708473	0.000010	1.506	0.006	190
		2/4/17	34.50	0.11	0.160	0.0016	314	0.708589	0.000009	1.497	0.004	123
		8/23/17	47.00	0.15	0.713	0.0071	313	0.708455	0.000010	1.499	0.005	235
НҮ9	Hyalite Creek below Lick Creek	8/23/17	8.52	0.04	0.039	0.0004	243	0.708590	0.000009	1.598	0.007	45
		12/14/ 17	11.8	0.05	0.080	0.0008	259	0.708532	0.000009	2.121	0.006	
HY16	Madison limestone spring channel	12/14/ 17	31.0	0.13	0.424	0.0042	233	0.708352	0.000009	5.226	0.017	
HY17	Madison limestone spring seep	12/14/ 17	26.9	0.12	0.038	0.0004	222	0.708349	0.000009	5.285	0.013	
		1/29/18	33.7	0.15	0.382	0.0038	228			5.282	0.032	
		3/27/18	32.9	0.15	0.372	0.0037	224	0.708357	0.000011	5.215	0.015	
HY10	Middle Hyalite Creek	8/23/17	11.00	0.04	0.079	0.0008	259	0.708602	0.000010	2.958	0.010	46
		12/14/ 17	14.5	0.05	0.114	0.0011	277	0.708574	0.000009	2.957	0.016	
HY11	Hyalite Creek at Langohr Logging Road	8/23/17	11.00	0.04	0.085	0.0009	259	0.708609	0.000009	2.966	0.008	49
HY13	Unnamed creek in glacial meadow	8/24/17	14.60	0.08	0.017	0.0002	192	0.708927	0.000009	1.961	0.058	88
HY12	Buckskin Creek	8/23/17	68.60	0.14	0.592	0.0059	504	0.711457	0.000009	2.695	0.228	212
HY4	Hyalite Creek at Langohr Campground	2/19/16	13.52	0.05	0.164	0.0016	261	0.708679	0.000009	3.195	0.009	
		8/25/16	12.50	0.05	0.069	0.0007	277	0.708661	0.000009	2.977	0.011	37
		2/4/17	17.60	0.06	0.186	0.0019	301	0.708679	0.000010	3.100	0.010	52
		8/23/17	11.40	0.04	0.088	0.0009	268	0.708789	0.000009	2.983	0.022	28
HY8	Moser Creek	2/4/17	37.10	0.14	0.596	0.0060	275	0.711434	0.000010	2.236	0.006	106
		8/23/17	47.10	0.16	0.542	0.0054	294	0.711809	0.000009	2.241	0.008	167
HY14	Hyalite Creek below Moser Creek	8/24/17	11.60	0.04	0.077	0.0008	267	0.708736	0.000009	3.047	0.012	45
HY15	Hyalite Creek above Practice Rock	8/24/17	11.60	0.04	0.083	0.0008	270	0.708847	0.000009	2.944	0.013	73
HY5	Hyalite Creek at Practice Rock	2/19/16	9.86	0.04	0.554	0.0055	246	0.711415	0.000010	1.788	0.005	
		8/25/16	12.60	0.05	0.170	0.0017	278	0.709791	0.000009	2.086	0.006	43
111/6	Healita Casal+ HOOG	8/24/17	11.90	0.04	0.152	0.0015	272	0.709734	0.000009	2.128	0.008	79
HY6	Hyalite Creek at USGS gauge 06,050,000	2/19/16	10.05	0.04	0.638	0.0064	249	0.712017	0.000010	1.691	0.005	
		8/25/16	12.70	0.05	0.121	0.0012	270	0.710067	0.000010	1.966	0.005	50
		2/4/17	14.40	0.05	0.791	0.0079	287	0.711124	0.000009	1.747	0.004	52
CD1	Coundariah Const	8/24/17	11.80	0.04	0.004	0.0000	274	0.709977	0.000009	2.047	0.010	61
SD1	Sourdough Creek	12/13/ 17	6.86	0.04	0.024	0.0002	181	0.708617	0.000009	2.047	0.018	07
GW2	Gneiss spring	5/18/17	15.30	0.05	0.353	0.0035	321	0.736865	0.000010	1.849	0.084	37
GW3 GW4	Gneiss well Hyalite Creek alluvial fan	5/18/17 6/20/17	27.00 42.90	0.06 0.11	0.364 0.233	0.0036 0.0023	467 383	0.744966 0.712214	0.000010 0.000010	1.489 1.784	0.022 0.006	146 139
GW4	well	0/20/1/	74.70	0.11	0.233	0.0023	303	0./12214	0.000010	1./07	0.000	139

<sup>\*</sup>Minimum detection limit (MDL).

# Square brackets denote activity ratios.

<sup>\*\*</sup> Alkalinity in units of mg  $CaCO_3$  equivalent per liter.

evaporated samples were re-dissolved in 0.6 mL of  $\sim 7$  N Optima<sup>TM</sup>-grade HNO<sub>3</sub>, transferred to acid-washed 2 mL centrifuge tubes, and centrifuged for 10 min at 10,000 rpm. Any solids were returned to the original Teflon vials and refluxed with concentrated, ultrapure HF and HNO<sub>3</sub>, were again evaporated, dissolved in 0.6 mL of  $\sim 7$  N Optima<sup>TM</sup> HNO<sub>3</sub>, and combined with the previously dissolved portion. Final solutions thus represent the total dissolved load present in water samples. Sr and U salts were separated and purified by standard ion exchange chemistry using AG1-X8 resin for the U fraction and Sr-Spec<sup>TM</sup> resin for the Sr fraction.

Purified U aliquots were loaded onto the evaporation side of a double rhenium filament assembly and analyzed by TIMS using the USGS SWIRL ThermoFinnigan Triton<sup>TM</sup> equipped with a single secondary electron multiplier and a retarding potential quadrapole (RPQ) electrostatic filter. Intensities of <sup>234</sup>U, <sup>235</sup>U, and <sup>236</sup>U were measured sequentially in dynamic peak-jumping mode. To correct for instrument bias and drift, the  $^{234}\text{U}/^{235}\text{U}$  values measured for unknowns were normalized by the same factor needed to adjust 234U/235U values measured for a NIST U-isotope standard (SRM 4231B) run in the same magazine to the accepted value of 0.007294 ( $\pm 0.000028$ ). One hundred fourteen analyses of SRM 4321B yielded an average  $^{234}\mathrm{U}/^{235}\mathrm{U}$  value of 0.007303 (0.007292 to 0.007314, 95% confidence interval), which is within error overlap of the NIST certified value. Measured  $^{234}$ U/ $^{235}$ U atomic ratios were converted to [234U/238U] using decay constants published by Cheng et al. (2013) ( $\lambda_{234} = 2.82206 \times 10^{-6} \text{ yr}^{-1}$ ) and Jaffey et al. (1971) ( $\lambda_{238} = 1.55125 \times 10^{-10} \text{ yr}^{-1}$ ) and the assumption that all U has an atomic <sup>238</sup>U/<sup>235</sup>U composition of 137.88 (Steiger and Jäger, 1977). Analytical errors for measured [ $^{234}$ U/ $^{238}$ U] are given at the 95% confidence level (i.e. twice the standard deviation) and include contributions from within-run counting statistics plus uncertainties propagated from blank, spike, and mass fractionation corrections, as well as external error derived from multiple analyses of the U isotope standard. Replicate analyses of a secondary standard consisting of 69.3-Ma uranium ore from the Schwartzwalder mine expected to be in radioactive secular equilibrium (i.e.,  $[^{234}\text{U}/^{238}\text{U}] = 1.000$ ; (Ludwig et al., 1985)) yielded an average  $[^{234}\text{U}/^{238}\text{U}]$  value of 0.9997  $\pm$  0.0032 (2  $\times$  standard deviation for 65 analyses). Total process blanks for U were typically 0.01-0.1 ng compared to total U abundances of 5-600 ng (median 85 ng). An in-house water "standard" developed by the USGS Branch of Quality Systems (SRS T-221) was processed multiple times at both MSU and SWIRL to evaluate interlaboratory biases. Results for [234U/238U] are identical within reported analytical uncertainty; however, U concentrations for aliquots processed at MSU are more scattered ( $\pm 7.7\%$ , 2  $\times$  SD, N = 4) with an average of 1.40  $\pm$  0.11 µg L<sup>-1</sup>, which is lower than the published most-probable-value of 1.49  $\pm$  0.08.

Purified Sr aliquots were loaded onto single rhenium filaments atop an initial load of tantalum oxide used as an activator and analyzed at the USGS SWIRL by multicollector TIMS using either a ThermoFinnigan Triton<sup>TM</sup> or an Isotopx Phoenix<sup>TM</sup>. Isotope measurements were made on 5 to 10 V 88Sr signals using multi-dynamic, triple-jump analytical routines where instrumental mass fractionation was corrected using <sup>86</sup>Sr/<sup>88</sup>Sr measured during the same run assuming a value of 0.1194. Replicate analyses of the National Institute of Standards and Technology Sr-isotope standard, SRM 987 (accepted <sup>87</sup>Sr/<sup>86</sup>Sr value of 0.710248; (McArthur et al., 2001)) used as a primary standard to normalized instrument bias and drift, yielded mean values of  $0.710250 \pm 0.000007$ ( $\pm 2 \times SD$ , N = 314) using the Triton<sup>TM</sup> and 0.710242  $\pm$  0.000012 ( $\pm 2 \times SD$ ) SD, N = 15) using the Phoenix<sup>TM</sup>. Measured  $^{87}$ Sr/ $^{86}$ Sr values for unknown samples were adjusted by the same amount needed to obtain the accepted value for NIST 987 analyzed during the same session. Replicate 87Sr/86Sr analyses of the modern-marine carbonate standard, EN-1 (accepted value of 0.7091741  $\pm$  0.0000024, (McArthur et al., 2006)), gave mean values of 0.709174  $\pm$  0.000008 ( $\pm$ 2 × SD; N = 174), and  $0.709176 \pm 0.000005$  ( $\pm 2 \times SD$ , N = 5) on respective instruments. Total process blanks for Sr were typically less than 0.001 µg compared to total Sr abundances of 20-140 µg (median 40 µg). Analytical errors for

 $^{87}\text{Sr}/^{86}\text{Sr}$  values are given at 95% confidence levels ( $\sim\!2\sigma$ ) and include within-run uncertainties and external error based on replicate analyses of standards. Results for  $^{87}\text{Sr}/^{86}\text{Sr}$  measured in SRS T–221 processed at MSU and SWIRL are identical within reported analytical uncertainty.

### 2.4. Isotope ratio and elemental ratio interpretation

We interpret the Sr isotope ratio as reflecting the isotopic character of weathered materials in contact with surface and groundwater, providing information about the mineralogical content and age of that weathered material. Differences in <sup>87</sup>Sr/<sup>86</sup>Sr in rocks and minerals depend on the isotopic composition of Sr at the time the rock formed as well as its Rb/Sr and age. Water interacting with solid materials during recharge and flow dissolves some of that Sr and incorporates the <sup>87</sup>Sr/<sup>86</sup>Sr ratio present in the lithologic source without significant isotopic fractionation. However, differences in weatherability of individual mineral components with variable Rb/Sr may result in a range of <sup>87</sup>Sr/<sup>86</sup>Sr values that reflect preferential dissolution of particular phases (White et al., 2005; Négrel et al., 2004; Pierret et al., 2014; Barbieri et al., 2005).

Along with <sup>87</sup>Sr/<sup>86</sup>Sr values, Ca/Sr mass ratios provide additional context for examining weathering and interaction of substrate and water (Hogan and Blum, 2003). Both Sr and Ca are divalent Group 2 alkaline earth metals of similar size, therefore they react similarly, allowing Sr to substitute readily for Ca in mineral lattices. During precipitation of carbonate minerals, Ca is preferentially incorporated into the crystal lattice, increasing the Ca/Sr in the solid and decreasing the Ca/Sr in remaining water (White et al., 2005).

We interpret the U activity ratios as reflecting the balance between preferential dissolution of <sup>234</sup>U derived from alpha decay of the parent isotope <sup>238</sup>U and bulk dissolution of U with from rock matrix that has a  $[^{234}\text{U}/^{238}\text{U}]$  near unity. This balance, in turn, is a function of the water/ rock interaction and integrates residence time, flow path length, chemical aggressiveness of weathering processes, and the ratio of exposed rock surface area to ambient volume of water. In rocks and minerals older than about 1 Ma, <sup>234</sup>U abundances reach a state of radioactive secular equilibrium with <sup>238</sup>U, meaning that the growth and decay of  $^{234}$ U become balanced with decay of  $^{238}$ U (half-life of 4.47  $\times$ 109 years) such that levels of radioactivity (rates of decay) for both isotopes are equal and the ratio of their activities equals unity (that is,  $[^{234}\text{U}/^{238}\text{U}] = 1.00$ ; Bourdon et al., 2003). Radioactive disequilibrium is a consequence of water-rock interaction, where alpha recoil occurring in the solid phase increases the susceptibility of <sup>234</sup>U to leaching relative to  $^{238}$ U, resulting in [ $^{234}$ U/ $^{238}$ U] values greater than one in the aqueous phase. The degree of [ $^{234}$ U/ $^{238}$ U] disequilibrium is a function of U concentration, particle surface area, water/rock ratios, chemical reactivity, and time (DePaolo et al., 2006; Maher et al., 2006). Higher [<sup>234</sup>U/<sup>238</sup>U] values reflect low water-rock ratios, longer flow paths allowing more exposure to recoil <sup>234</sup>U, or greater mineral surface areas interacting with a given volume of water (Bourdon et al., 2003; Chabaux et al., 2003; Suksi et al., 2006; Dosseto et al., 2008; DePaolo et al., 2012). However, increases in [234U/238U] values are limited by rates of weathering and bulk rock dissolution, which drive [234U/238U] values back towards unity (Maher et al., 2006).

Isotopes of Sr and U allow identification of end members because their ratios are usually not affected by dilution or near-surface physical or chemical processes other than those of interest here (Paces and Wurster, 2014). One exception to this could be contexts where reducing conditions favor loss of dissolved  $\rm U^{6+}$  to precipitation with reduction to  $\rm U^{4+}$ , such as in a wet meadow environment rich in organic matter where water flow is slowed. This loss of U could lead to erroneously low estimation of contribution from an endmember characterized upgradient of such an environment, and might be evident in skewed concentration relationships. Thus, care must be taken to appropriately characterize end members, acknowledge geomorphic context, and recognize effects of U loss through chemical reduction. In Hyalite Canyon, these wet

meadow environments occur in the glaciated middle and upper reaches of the canyon, above HY4. One spring-fed wet meadow was sampled, at site HY13.

As a complement to these primary geochemical measures, we used  $^{222}\mathrm{Rn}$  activities to qualitatively establish the broader range of subsurface inflows to Hyalite Creek (Hoehn et al., 1992). Concentrations of  $^{222}\mathrm{Rn}$  reflect the  $^{238}\mathrm{U}$  decay series in the form of this short-lived intermediate with a half-life of 3.8 days. This short half-life allows quantification of residence times from days to weeks in groundwater (Schubert et al., 2006), whereas older groundwater will simply be equilibrated with  $^{222}\mathrm{Rn}$  efflux in the aquifer. Because Rn is a noble gas, air–water exchange rapidly depletes concentrations in surface water, making detection of elevated  $^{222}\mathrm{Rn}$  a useful tracer of all groundwater inflows older than days (Gardner et al., 2011).

### 2.5. Data interpretation

We interpreted patterns in stream flow generation from groundwater aquifers along Hyalite Creek first by examining the longitudinal patterns in chemical and isotope characterizations with decreasing elevation and distance downstream. Longitudinal analysis allowed consideration of how geologic structures, geomorphology, and lithology influence the character of stream flow generation and surface–subsurface water interaction (Gardner et al., 2011). This sampling strategy allowed us to construct mixing models that quantify fractional inputs of groundwater to reaches of Hyalite Creek where geochemical data indicated notable influence of a given aquifer.

Two mixing analyses were performed to estimate the fraction of stream flow that could be attributed to chemically distinguishable aquifers along Hyalite Canyon. A binary mixture (*M*) can be calculated from concentrations (*C*), isotopic ratios (*R*), and fractional contributions (*f*) from each of two end members. In this case the two end members are the water at the upstream end of a reach (A) and the water contributed from a given groundwater source along the reach (B) that together constitute the mixture (*M*) at the downstream end of the reach (Faure and Mensing, 2005; Arendt et al., 2015):

$$C_M = C_A f_A + C_B f_B \tag{1}$$

$$R_{M} = R_{A}f_{A}\left(\frac{C_{A}}{C_{M}}\right) + R_{B}f_{B}\left(\frac{C_{B}}{C_{M}}\right)$$
 (2)

where  $f_A + f_B = 1$ . Here, we identify hydrologic end members and evaluate mixtures of end members defined by Sr concentration,  $^{87}$ Sr,  $^{86}$ Sr, U concentration, and  $[^{234}$ U/ $^{238}$ U], so Eqs. (1) and (2) were repeated for Sr and U and solved simultaneously.

Rather than evaluate the entire stream system, we used the binary mixing model and Monte Carlo analysis to estimate groundwater inputs to Hyalite Creek over two reaches where groundwater inputs from two distinctive aquifers (karst flow in Madison Group limestones and fracture flow in Archean gneiss) are particularly likely to influence stream compositions. While there are numerous tributaries and other small inputs of water to Hyalite Creek, we refined our sampling to capture the two distinct reaches of Hyalite Creek where groundwater inputs from these sources can be quantified without the potentially confounding effects of surface inflow. The upper to middle elevations of Hyalite Creek were characterized as a two end member mixture between surface water discharging from Hyalite Creek below Hyalite Reservoir (site HY7, 1962 m, representing water having interacted with clastic sedimentary rock and volcanics in the upper part of the catchment), and groundwater input from the Madison aquifer (sites HY16 and HY17; 1931-1936 m). The resulting mixture below the presumed influence of the Madison inflows was sampled at site HY10 (1909 m) during August 2017 baseflow conditions. A second two-component end member mixing model uses surface waters of middle Hyalite Creek below the influence of the Madison (sites HY14 and HY15; 1854 m) and groundwater from the

Archean gneiss sampled in Hodgeman's Canyon (sites GW2 and GW3). The resulting mixture below the presumed influence of Archean Gneiss inflows was sampled at site HY5 (1807 m) during both August and February baseflow conditions.

For a given mixing reach and end member definition, we solved Eqs. (1) and (2) simultaneously for U and Sr using a numerical iterative optimization scheme. The optimization goal was to find the combination of  $f_A$  (upstream end member) and  $f_B$  (groundwater end member) for the mixing model that would have the maximum likelihood of matching the observed concentrations and isotope ratios for both Sr and U at the downstream end of the reach. We used R statistical software and the optim() function from the base R stats package to find the maximum likelihood estimate (i.e. MLE analysis) based on the quasi-Newton L-BFGS-B algorithm (Ewing et al., 2020). Likelihood for the MLE was calculated based on the assumption that the residual errors between the modeled mixture values and the observed mixture values were independent and normally distributed (Ewing et al., 2020). The assumed standard deviations of the residual errors necessary for calculating the likelihood in this fashion were based on estimates of analytical uncertainty of each end member in the overall sample analysis.

We estimated the effect of uncertainty in end member concentrations and isotope ratios on the MLE-inferred composition of a given observed mixture using a Monte Carlo analysis. We characterized uncertainty for each end member using a random variable with a normal distribution, estimated from multiple samples characterizing that end member over time and similar sites sampled on the same date. We then generated an ensemble of 5,000 realizations of the inferred composition for a given observation, where each realization was generated by randomly sampling from the normal distributions defining the uncertainty in the end members and repeating the MLE. Normal distributions truncated at zero were used to characterize uncertainty in end members, such that nonsensical results were excluded from the ensemble results. The 95% confidence intervals of the ensemble results are reported based on the 2.5 and 97.5 percentiles of the 5,000 realizations.

Equation (2) describes two end member mixing using an isotopic system with distinct compositions for each end member. However, many hydrologic situations are more complex and involve mixtures of more than two end members. In these situations, the use of a single isotope-system may not be sufficient to discriminate between multiple end members. Recent studies evaluated simple three end member mixing using the two independent U and Sr isotope systems to determine contributions of different hydrologic sources with distinct radiogenic isotope signatures (Drexler et al., 2014; Paces and Wurster, 2014). We follow this general approach in lower Hyalite Canyon, where we consider whether inmixing of Archean gneiss derived water can explain the observed isotopic values.

### 3. Results

#### 3.1. U and Sr concentrations

Concentrations of dissolved Sr and U in the main stem of Hyalite Creek tend to increase downstream as elevation decreases (Table 3, Fig. 3a). Concentrations of Sr increase from 0.02 to 0.03 mg L $^{-1}$  in the upper elevations of Hyalite Creek (sites HY1 and HY2) to 0.04–0.05 mg L $^{-1}$  at lower elevations (sites HY5 and HY6). Much of this increase occurs over the reach where the stream valley intersects Mesozoic sedimentary rocks, particularly from sites HY7 to HY10. Further downstream, Hyalite Creek intersects older geologic units including Paleozoic carbonate rocks between sites HY10 and HY4. Sr concentrations in the main stem remain more-or-less constant between 0.04 and 0.06 mg L $^{-1}$  over this middle reach and into the lower reach, which cuts through Archean gneiss at sites HY14, HY15, HY5, and HY6. Samples from tributary watersheds draining Mesozoic and Paleozoic sedimentary rocks tend to have higher and more variable Sr concentrations (0.08 to 0.16 mg L $^{-1}$ ). Groundwater sampled from wells or springs hosted in the Archean gneiss

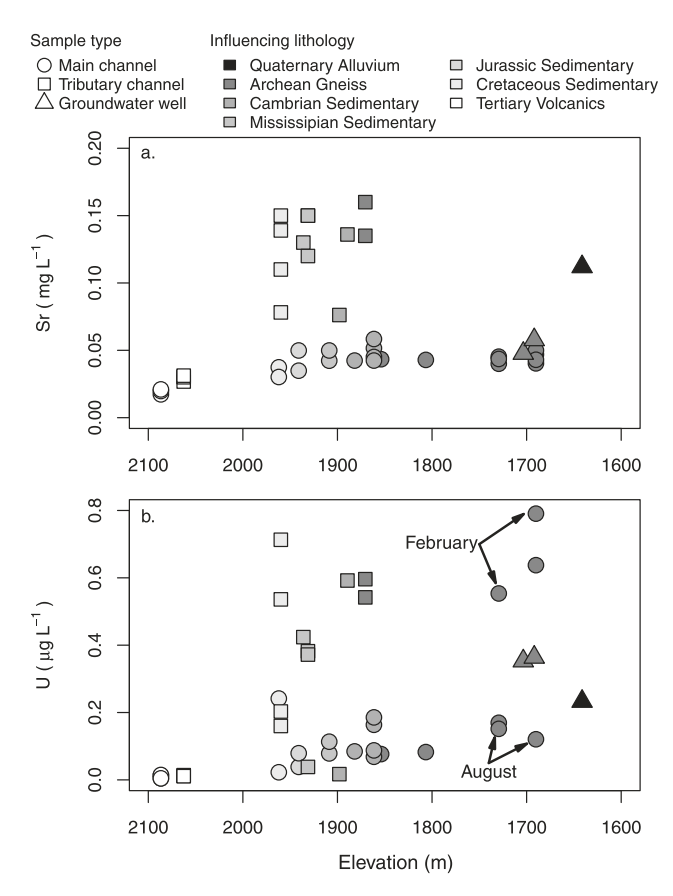


Fig. 3. Strontium and uranium concentrations in water samples plotted against elevation in Hyalite Canyon. Sr (mg  $L^{-1}$ ) (a) and U ( $\mu$ g  $L^{-1}$ ) (b) were measured in water samples collected from the main channel of Hyalite Creek (circles), its tributaries (squares), and nearby wells (triangles). Greyscale fill shades indicate the lithology present at the sample site. Arrows indicate seasonal differences in lower Hyalite Canyon.

from Hodgman's canyon (GW2 and GW3) has Sr concentrations similar to those of the lower reaches of Hyalite Creek (0.05 to 0.06 mg L'). The alluvial aquifer well sample at the mouth of Hyalite Canyon has a higher Sr concentration (0.11 mg  $\rm L^{-1})$  than samples of Hyalite Creek at the mountain front. Overall, Sr concentrations did not vary systematically among sampling dates at any given site.

Concentrations of U followed trends similar to Sr concentrations, and generally increased with distance downstream in the main stem of Hyalite Creek (Table 3, Fig. 3b). U concentrations varied between 0.005 and 0.015 μg L<sup>-1</sup> at higher elevations (sites HY1 and HY2), where Hyalite Creek drains Tertiary volcanic rock. Again, much of the longitudinal increase in concentration occurred in the middle elevations of Hyalite Creek (sites HY7 to HY4), coinciding with the inflow of springs and tributaries that tend to have higher and more variable U concentrations  $(0.017 \text{ to } 0.713 \text{ } \mu\text{g L}^{-1})$  than the main stem  $(0.023 \text{ to } 0.242 \text{ } \mu\text{g L}^{-1})$ . Samples from a given site collected in February and August had similar U concentrations for most sites (HY1-HY4, HY7-HY17). However, concentrations of U in main stem samples from the lower elevations of Hyalite Creek (HY5, HY6) were substantially higher in February (0.544 to 0.791  $\mu$ g L<sup>-1</sup>) than in August (0.121 to 0.170  $\mu$ g L<sup>-1</sup>). The groundwater from Hodgman Canyon wells (sites GW2 and GW3) is presumed to reflect the influence of gneiss, and had U concentrations in the range of 0.353 to  $0.364~\mu g~L^{-1}$ , which was near the middle of the range observed in samples from sites HY5 and HY6. The upper alluvial fan well (GW4) had a U concentration of 0.233 µg L<sup>-1</sup>, intermediate between those of February and August samples from Hyalite Creek at the mountain front.

#### 3.2. Ca/Sr ratios

Ratios of Ca/Sr along Hyalite Creek follow patterns similar to those observed for Sr and U concentrations (Table 3). Values in the main stem tend to gradually increase with distance downstream from values between 170 and 200 in upper Hyalite Creek (sites HY1 and HY2) to values between 250 and 290 in the lower canyon (HY5 and HY6). Much of this shift occurs over the transition from areas underlain by Tertiary volcanic rock to Mesozoic sediments (sites HY7 and HY9). Values continue to increase in the middle elevations of the main stem between sites HY10 and HY14, reflecting inputs from Paleozoic carbonate units in this reach. Ca/Sr values remain constant as the main stem cuts through Archean gneiss (sites HY15, HY5, and HY6), although some seasonal variation between February and August sampling events is notable in lower canyon samples. Tributary samples at middle elevations show greater variability (both higher and lower values). In contrast to main stem water, Archean gneiss wells (sites GW2 and GW3) have high Ca/Sr ratios of 321 and 467. The well in the alluvial fan aquifer at the mouth of Hyalite Canyon also has a much higher Ca/Sr value (383) than samples of Hyalite Creek water at the mountain front (249-297). Trends in alkalinity are similar to those in Ca/Sr (Table 3), with higher values in tributaries draining Mesozoic and Paleozoic sedimentary rock units and gradually increasing values in main stem samples downstream of confluences with tributaries draining sedimentary rock units. None of the sites demonstrated systematic variations in Ca/Sr among sampling dates.

### 3.3. Sr isotope ratios ( $^{87}Sr/^{86}Sr$ )

Inflections in <sup>87</sup>Sr/<sup>86</sup>Sr values along the main stem of Hyalite Creek also align with transitions in parent bedrock along the valley (Tables 2 and 3, Fig. 4). Values for  ${}^{87}$ Sr/ ${}^{86}$ Sr range from 0.70883 to 0.70921 in the upper reaches draining Tertiary volcanic bedrock (sites HY1 and HY2). <sup>87</sup>Sr/<sup>86</sup>Sr ratios in main stem samples decrease to values of 0.70853 to 0.70871 below Hyalite Reservoir (site HY7) through areas draining Mesozoic and Paleozoic marine mudstones, shales, and limestones at intermediate elevations (sites HY9 through HY11). Tributaries and springs along this reach (sites HY3, HY16 and HY17) contribute somewhat lower <sup>87</sup>Sr/<sup>86</sup>Sr values ranging from 0.70835 to 0.70859. Tributaries draining sub-basins containing mixtures of Paleozoic sediments (sites HY13 and HY12) and Archean gneiss (site HY8) have elevated <sup>87</sup>Sr/<sup>86</sup>Sr values ranging from 0.70893 to 0.71181. Main stem samples have <sup>87</sup>Sr/<sup>86</sup>Sr values that increase marginally through this reach where bedrock transitions from Paleozoic sedimentary rock to Archean gneiss to values of 0.70866 to 0.70885. Unlike Sr concentrations, <sup>87</sup>Sr/<sup>86</sup>Sr values for sites at higher or middle elevations showed minimal differences among sample dates.

Main stem samples in the lower reach of Hyalite Creek have higher  $^{87}\mathrm{Sr}/^{86}\mathrm{Sr}$  values ranging from 0.70973 to 0.71202, coinciding with the intersection of the valley with Archean gneiss bedrock (sites HY5 and HY6, Fig. 4). Groundwater samples from wells in the Archean gneiss (sites GW2 and GW3) have substantially higher <sup>87</sup>Sr/<sup>86</sup>Sr compositions of 0.73687 and 0.74497 (Table 3). In addition, <sup>87</sup>Sr/<sup>86</sup>Sr in main stem samples from sites in lower Hyalite Canyon (HY5 and HY6) show substantial variation among sample dates, with the highest values observed in February during the lowest flows, and the lowest values observed in August during somewhat higher flows (overall range of 0.70973 to 0.71202). Furthermore, <sup>87</sup>Sr/<sup>86</sup>Sr values in samples of main stem water at the canyon mouth (site HY6) were consistently higher than water sampled upstream (site HY5) during each sampling campaign. Values of  $^{87}\mathrm{Sr}/^{86}\mathrm{Sr}$  in August streamflow at HY6 were much lower than those measured in the June 2017 sample of well water from the alluvial fan near the mouth of the canyon (site GW4; values of (0.71007 to 0.70998 versus 0.71221, respectively). However, the elevated  $^{87}$ Sr/ $^{86}$ Sr value for HY6 streamflow sampled in February 2016 (0.71202) was similar to GW4 groundwater.

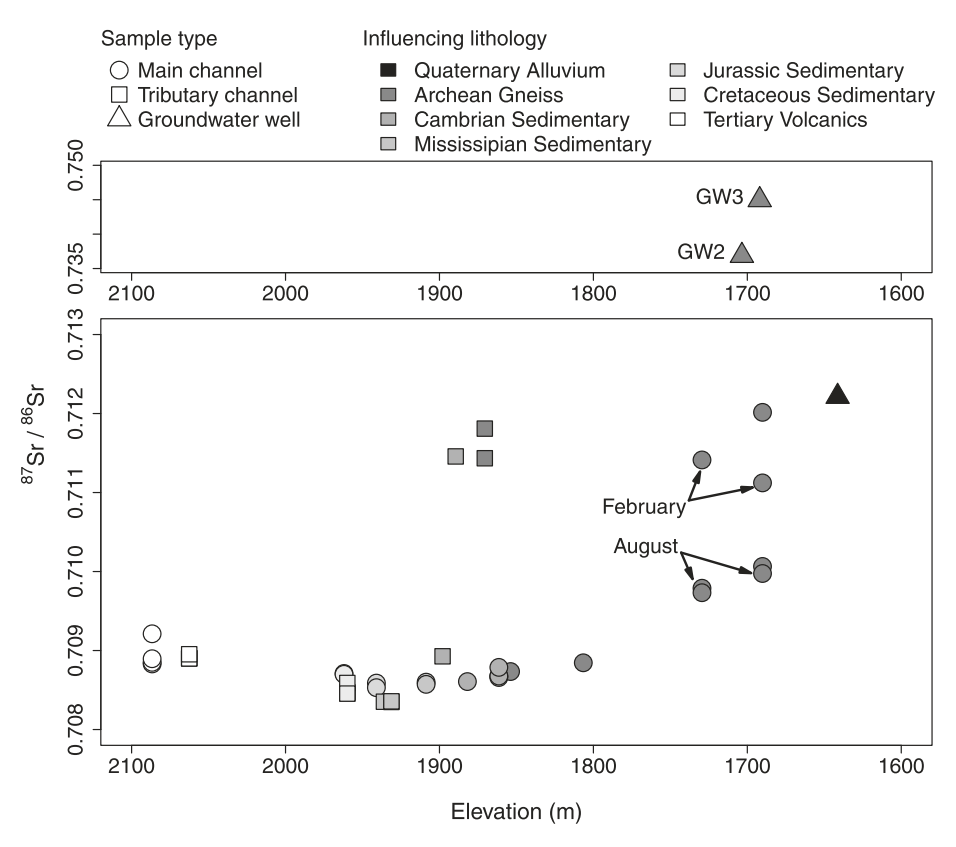


Fig. 4. <sup>87</sup>Sr/<sup>86</sup>Sr values in water samples plotted against elevation in Hyalite Canyon. Greyscale fill indicates the lithology present at the sample site, and shape indicates sample type. Groundwater samples from wells in Hodgman Canyon (GW2, GW3) have particularly high values consistent with their Archean gneiss host lithology. Arrows indicate seasonal differences in lower Hyalite Canyon.

### 3.4. Uranium activity ratios ( $[^{234}U/^{238}U]$ )

Samples of Hyalite Creek headwaters (sites HY1 and HY2) as well as water from immediately below Hyalite Reservoir (HY7) have relatively

low and uniform [ $^{234}$ U/ $^{238}$ U] values ranging from 1.59 to 1.72 (Table 3, Fig. 5). In contrast, water discharging from the Madison aquifer at sites HY16 and HY17 has much higher [ $^{234}$ U/ $^{238}$ U] values of 5.23 and 5.29. Values for [ $^{234}$ U/ $^{238}$ U] in stream water increase to between 2.94 and

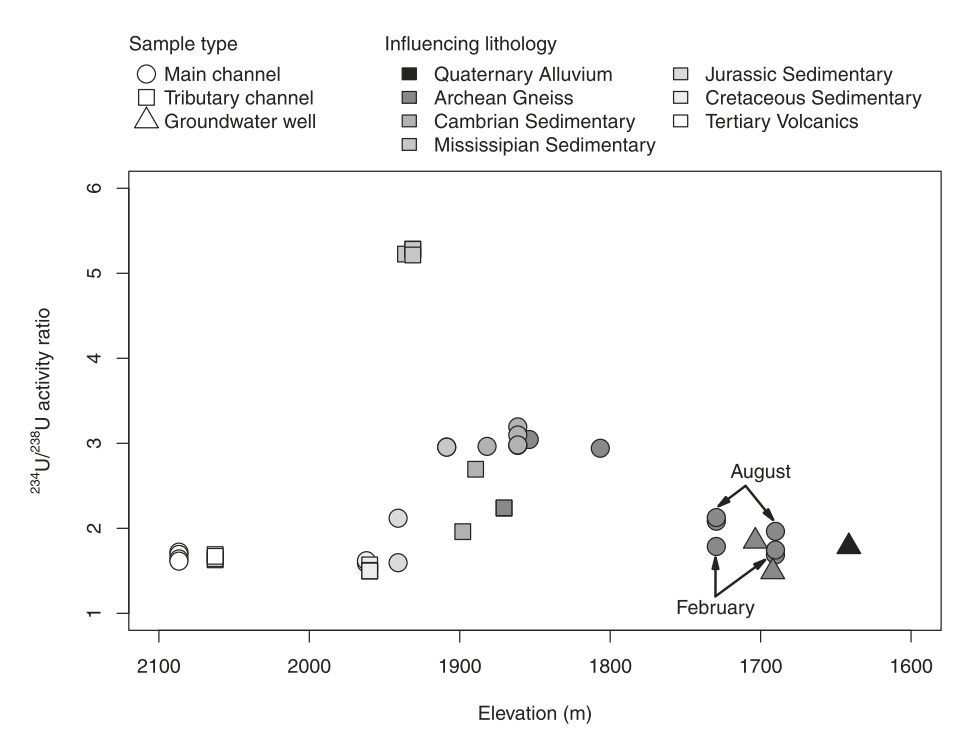


Fig. 5. [234U/238U] values (activity ratios) in water samples plotted against elevation in Hyalite Canyon. Greyscale fill indicates the lithology present at the sample site, and shape indicates sample type. Arrows indicate seasonal differences in lower Hyalite Canyon. Site locations are shown in Fig. 1.

3.20 over the intermediate elevations, where the Hyalite Creek valley intersects Madison aquifer bedrock (sites HY10 and HY11), and the reach immediately downstream (sites HY4, HY14, HY15). Water from tributary watersheds draining sedimentary rocks along the same reach (sites HY3, HY12, HY13, and HY8) shows a wide range of [ $^{234}$ U] values from 1.50 to 2.69.

Main stem samples of lower Hyalite Creek (sites HY5 and HY6) have distinctly lower [ $^{234}$ U/ $^{238}$ U] values (1.69 to 2.13) relative to those at intermediate elevations, reflecting a progressive decrease as Hyalite Creek cuts through Archean gneiss. Values of [ $^{234}$ U/ $^{238}$ U] in lower Hyalite Creek are similar to those in groundwater sampled from wells drilled in Archean gneiss (GW2 and GW3; 1.85 and 1.49). Differences in [ $^{234}$ U/ $^{238}$ U] at a given site are only apparent at sites HY4, HY5, and HY6. February samples from site HY4 displayed higher [ $^{234}$ U/ $^{238}$ U] values than August samples, while February samples from sites HY5 and HY6 displayed lower [ $^{234}$ U/ $^{238}$ U] values compared to August samples. Values of [ $^{234}$ U/ $^{238}$ U] in lower Hyalite Creek are also comparable to those in groundwater sampled from alluvium along the mountain front near the mouth of Hyalite Canyon (GW4; 1.78).

#### 3.5. Estimates of fractional groundwater contributions

Variations in isotopic ratios across the full sample set were evaluated in <sup>87</sup>Sr/<sup>86</sup>Sr vs. [<sup>234</sup>U/<sup>238</sup>U] space as a mixture of three end members defined by compositions derived from water/rock interactions with Archean gneiss, Madison Group limestones, and Absaroka volcanics (Fig. 6). Progression of Hyalite Creek Sr and U isotopic ratios within the curved space defined by mixing models between the three end members provides a graphic perspective on the cumulative influence of aquifers with distance downstream. Concentrations of binary mixtures (equation (1)) will result in fractional contributions (f) that are distributed equally along a straight line between end member compositions. However, isotopic compositions of binary mixtures depend on both concentrations and isotope ratios of both end members (equation (2)). As a result, the end member with the higher concentration more strongly influences the isotopic ratio of the mixture. If concentrations of the end members are not equal, this nonlinearity results in a hyperbolic mixing curve with non-equal spacings of fractional contributions when isotopic ratios are plotted (Faure and Mensing, 2004). Mixing end members are

represented by (1) average values for samples from upper Hyalite Creek that have interacted mainly with Absaroka volcanics and Cretaceous siliciclastic sediments (sites HY1, HY2, HY3, HY7, and HY9), characterized by low  $^{87}\mathrm{Sr/}^{86}\mathrm{Sr}$  and  $[^{234}\mathrm{U/}^{238}\mathrm{U}]$  values; (2) Madison aquifer spring water (HY16, HY17), characterized by low  $^{87}\mathrm{Sr/}^{86}\mathrm{Sr}$  and high  $[^{234}\mathrm{U/}^{238}\mathrm{U}]$  values; and (3) well water drawn from Archean gneiss (GW2, GW3), characterized by high  $^{87}\mathrm{Sr/}^{86}\mathrm{Sr}$  and low  $[^{234}\mathrm{U/}^{238}\mathrm{U}]$  values. We used these end member values to define a mixing web, where we then plotted sample isotopic compositions (Fig. 6).

Loads of Sr and U in the upper reaches of Hyalite Creek are presumed to be derived primarily from interactions with Eocene Absaroka volcanic rocks, hence the use of their average  $^{87}\mathrm{Sr}/^{86}\mathrm{Sr}$  and  $[^{234}\mathrm{U}/^{238}\mathrm{U}]$  compositions to define the volcanic end member. The isotopic composition of main stem stream waters at intermediate elevations differs from the Eocene volcanic end member primarily in  $[^{234}\mathrm{U}/^{238}\mathrm{U}]$ , and diverges from the volcanic end member along a binary mixing curve defined by Eocene volcanic and Madison aquifer end members (the lower boundary of the ternary mixing web in Fig. 6). Mixing relations between these two end members suggest that groundwater from the Madison aquifer contributes about 4% of stream flow at intermediate elevations along Hyalite Creek.

Where the Hyalite Creek valley intersects Archean gneiss bedrock,  $^{87}$ Sr/ $^{86}$ Sr values in main stem samples increase and [ $^{234}$ U/ $^{238}$ U] values decrease. Groundwater in Archean gneiss has low [234U/238U] values similar to water associated with Eocene volcanic rock, but much higher <sup>87</sup>Sr/<sup>86</sup>Sr values than water associated with Eocene volcanic rock (i.e. from a more radiogenic source). Compositions of main stem water at lower elevations progressively diverge from the volcanic-Madison limb of the mixing web (Fig. 6). This divergence trends towards the gneiss end member and away from the Madison end member in three-end-member space. When stream flows were lowest in February, main stem samples closest to the mouth of the canyon (HY5 and HY6) approach the binary mixing curve defined by Eocene volcanics and Archean gneiss (left boundary of mixing web). Based on models of mixing between the three end members, streamflow at the mouth of Hyalite Canyon (HY6) during February sampling was composed of up to 6% water influenced by Archean bedrock, with very little signature left from water influenced by Madison limestones (i.e., less than 1% contribution).

Two-component mixing relations were also evaluated using a Monte

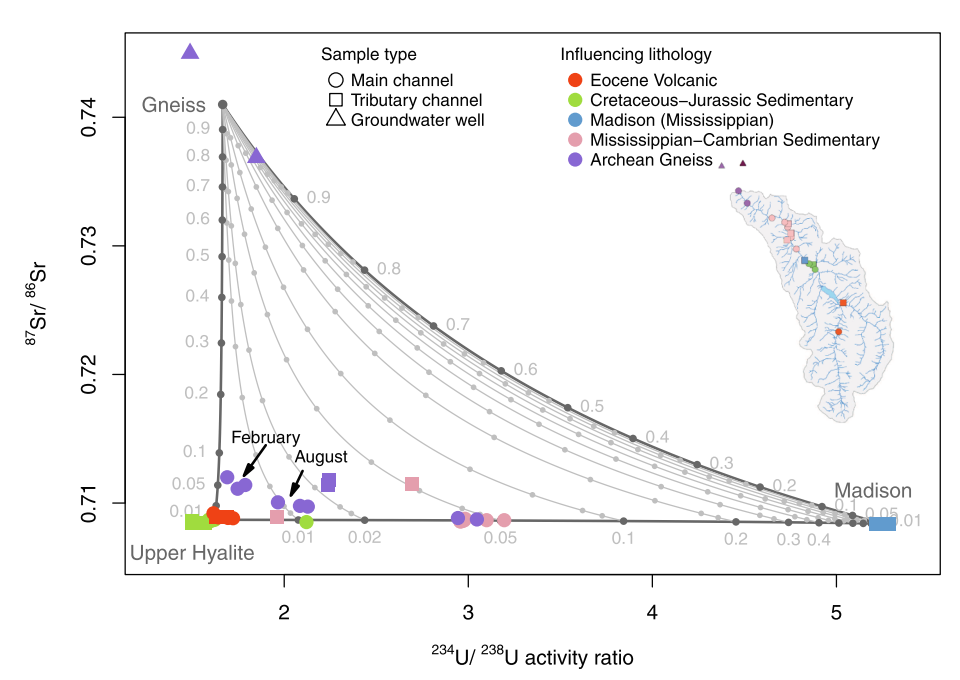


Fig. 6. Mixing models for Hyalite Canyon data. Srand U-isotopic compositions of mainstem and tributary samples fall inside a mixing web with three end members defined as water having interacted with Tertiary volcanic/Mesozoic sedimentary rocks (Upper Hyalite), Madison Group limestone (Madison), and Archean quartzofeldspathic gneiss (Gneiss). Numbered dots on each binary mixing limb are fractional contributions ranging from 0 to 1. Grey lines inside the web represent binary mixtures between the gneiss end member and fractional mixtures of Upper Hyalite plus Madison waters. Inset location map depicts sample origin based on contributing lithology. Seasonal difference in gneiss-influenced stream water samples collected in February and August is indicated.

Carlo uncertainty analysis of optimized mixing models, providing perspective on the degree to which groundwater aquifers are likely contributing to Hyalite Creek at two locations along the canyon and during two seasons (Fig. 7) (Ewing et al., 2020). Groundwater contributions from the Madison aquifer (HY16, HY17) with elevated [<sup>234</sup>U/<sup>238</sup>U] values (5.21–5.29) and low <sup>87</sup>Sr/<sup>86</sup>Sr values (0.70835–0.70836) cause a shift of compositions in main stem samples between upstream (HY7) and downstream (HY10) sites from 1.62 to 2.96 for [<sup>234</sup>U/<sup>238</sup>U] and from 0.70870 to 0.70860 for <sup>87</sup>Sr/<sup>86</sup>Sr. Based on the ensemble of mixing optimizations for net gains over this reach (Fig. 7a)(Ewing et al., 2020), we estimate that the Madison Group limestone aquifers contributed approximately 3.7% of the streamflow at site HY10 during baseflow conditions in August 2017 (reported as the median of the ensemble with a 95% confidence interval of 0.3% to 8.7%).

A two-end-member mixing model was also used to access contributions from the Archean gneiss aquifer during baseflow conditions in August 2017 and February 2017 (Fig. 7b and c) (Ewing et al., 2020). For the August 2017 model, average values from sites HY14 and HY15 are

assumed to represent the end member at the upstream end of the mixing reach, with higher  $[^{234}\text{U}/^{238}\text{U}]$  values (2.94 to 3.05) and lower  $^{87}\text{Sr}/^{86}\text{Sr}$ values (0.70874 to 0.70885) relative to the downstream end of the mixing reach at site HY5. Isotopic ratios for the Archean aquifer end member estimated from wells GW2 and GW3 have [234U/238U] values of  $1.49 \text{ to } 1.85 \text{ and } ^{87}\text{Sr/}^{86}\text{Sr values of } 0.73687 \text{ to } 0.74497. \text{ Mixing of main}$ stem flow with groundwater or runoff inputs over the reach resulted in downstream isotopic ratios (at HY5) of 2.13 for [234U/238U] and 0.70973 for  $^{87}\text{Sr}/^{86}\text{Sr}.$  The ensemble of mixing optimizations for these reaches suggests that the Archean aquifers contributed approximately 10.9% of the streamflow at site HY5 during baseflow conditions in August 2017 (reported as the median of ensemble with 95% confidence interval of 7.4% to 16.2%, Fig. 7b) (Ewing et al., 2020). However, the isotopic compositions of the downstream site fall outside the ensemble of the mixing models (HY5), indicating that Sr and U isotopes are providing conflicting information about the contribution of the two purported end members.

For the February 2017 model, the sample from middle Hyalite Creek at site HY4 (located below the main influx of water from the Madison

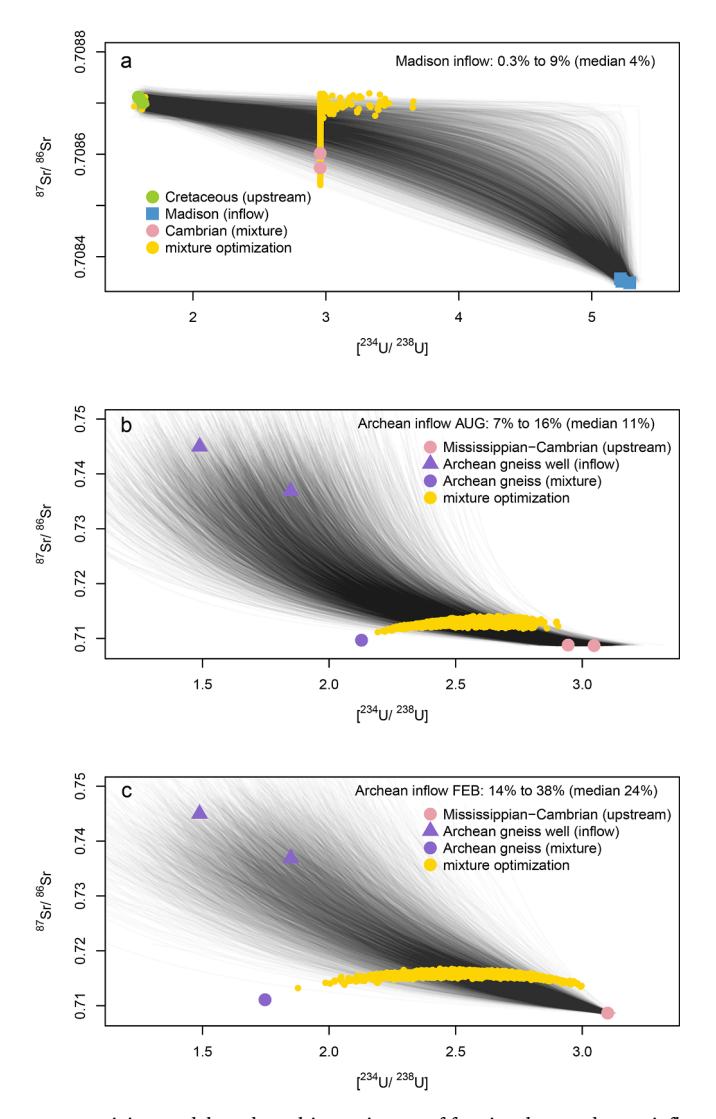


Fig. 7. Monte Carlo ensembles of two-component mixing models and resulting estimates of fractional groundwater inflows to Hyalite Creek. Inflows are estimated for discreet segments of Hyalite Creek from: (a) the Madison group limestone aquifer at 1920 m elevation in August 2017; (b) the Archean gneiss aquifer in lower Hyalite Canyon in August 2017; and (c) the Archean gneiss aquifer in February 2017. Each semi-transparent black line represents a single realization of a two-component mixing model based on a random sampling from the estimated uncertainty in each of two end members. Overlap of the semi-transparent lines results in darker areas that probabilistically represent the more likely regions of the potential mixing space if the end members and uncertainties are accurate. Gold circles represent realizations of each optimized fraction of aquifer contribution corresponding to each mixing line realization. Source code and fractional contribution density plots are provided in Ewing et al. 2020.

aquifer and above the exposed gneiss) was used as the upstream end member, because sites HY14 and HY15 were not sampled on that date. For the mixture site HY6 was used instead of HY5, as site HY5 was not sampled in February of 2017. Compared to HY14 and HY15 on other dates, HY4 in February 2017 has a higher  $[^{234}U/^{238}U]$  value (3.01) and lower <sup>87</sup>Sr/<sup>86</sup>Sr value (0.70868) consistent with Madison influence. The same gneiss end member (GW2 and GW3) was used in the February 2017 model. As simulated in August, the influence of gneiss groundwater would decrease the [234U/238U] value and increase the 87Sr/86Sr value of Hyalite Creek, which is consistent with the decreased  $[^{234}U/^{238}U]$  value of 1.75 and increased  $^{87}Sr/^{86}Sr$  value of 0.71112 observed at site HY6. We therefore model HY6 as a mixture between (1) waters of middle Hyalite Creek (HY4), and (2) water derived from the Archean gneiss as represented by GW2 and GW3 (Fig. 7c). Using these values in our mixing optimization, we estimate that fracture flow from the Archean gneiss contributes a median of 24.2% (95% confidence interval 14.3% to 37.5%, Fig. 7c and Ewing et al. 2020) of streamflow to lower Hyalite Creek (HY6) during February baseflow conditions. However, the Sr and U isotope ratios again provide conflicting information about end member contributions.

Using the same Monte Carlo realization and optimization model we also evaluated the Sr data alone as an indicator of Archean gneiss influence, without including U data. This approach is based on the sensitive response of this tracer to the Archean endmember. Using only Sr isotopic composition and concentration data, we estimate that a median of 2.4% (95% confidence interval 1.6% to 4.1%) of water in lower Hyalite Creek can be attributed to inflows from the Archean gneiss over the targeted reach during baseflow conditions in August and a median of 8.4% (95% confidence interval of 4.9% to 14.6%) of water can be attributed to Archean gneiss inflows in February (see Ewing et al. 2020).

Absolute fluxes of water relative to measured discharge at the downstream gauge sites can also be estimated from mixing model results. Given the percentage estimates calculated in the preceding paragraphs, additions to main stem streamflow from Archean sources are estimated at 0.17 m $^3$  s $^{-1}$ , or 11% of the total 1.57 m $^3$  s $^{-1}$  measured at site HY6 in August 2017. A similar influx of 0.14 m $^3$  s $^{-1}$  is estimated for February 2017 data (24% of 0.60 m $^3$  s $^{-1}$ ). If the Sr results alone are used,

estimated inflows are 0.038 m³ s $^{-1}$  (2.4%) in August, and 0.050 m³ s $^{-1}$  (8.4%) in February 2017. Additions to streamflow from Madison sources in the middle reaches of Hyalite Creek are estimated at 0.04 m³ s $^{-1}$ , or 3.7% of the total 1.14 m³ s $^{-1}$  measured at site HY7 in August 2017. The longitudinal assay of  $^{222}$ Rn activities indicates more widespread

The longitudinal assay of <sup>222</sup>Rn activities indicates more widespread groundwater influence than our geochemical indicators specific to the Madison and Archean waters (Fig. 8). Positive (nonzero) values indicate subsurface inflows older than days to weeks, which are evident at all sites other than HY7. The location of HY7 just below Hyalite Reservoir provides a measure of water that is completely degassed, as expected. Groundwater inflows (HY16 and HY17), mid-elevation tributaries (HY3 and HY8), and the high elevation main stem site (HY1) all have comparable <sup>222</sup>Rn levels (~20–40 pCi L<sup>-1</sup>), suggesting that our quantitative point measures provide snapshots of host-specific, older groundwater influence that is only a portion of the groundwater spectrum influencing streamflow.

#### 4. Discussion

Longitudinal evaluation of Ca, Sr, U and Rn dissolved in stream and ground waters provide a multifaceted means of assessing the nature of baseflow generation along Hyalite Canyon. Data in this study track the compositional evolution of streamflow caused by contributions from groundwater or tributary flow that reflect weathering of soils and rocks of varying lithology, allowing useful hydrologic inferences for local streamflow generation throughout the Hyalite Creek watershed.

### 4.1. Values for <sup>87</sup>Sr/<sup>86</sup>Sr in regional rocks and waters

Previous studies have determined <sup>87</sup>Sr/<sup>86</sup>Sr values for a number of rock units and streams in the region (Table 2). These values provide constraints on how variations in lithology across the Hyalite Creek watershed are likely to influence <sup>87</sup>Sr/<sup>86</sup>Sr values observed in stream flow. The range of <sup>87</sup>Sr/<sup>86</sup>Sr values that we observed in Hyalite Canyon waters (0.7089–0.7450) is consistent with the variety of host rock units present, though mixing processes likely restrict these values relative to primary source waters.

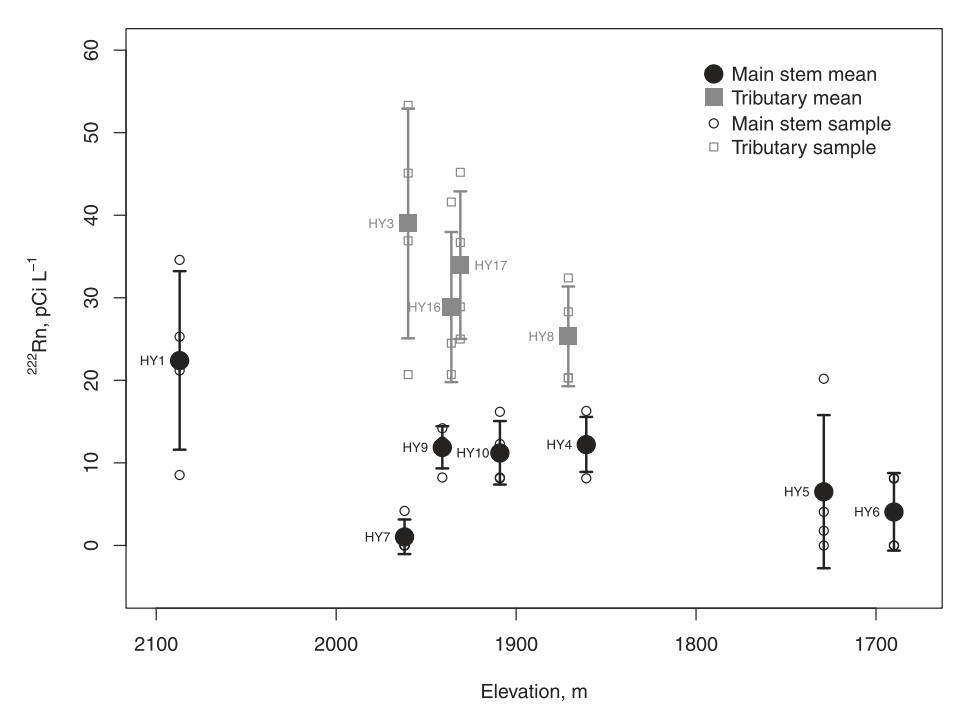


Fig. 8. Means and point observations of <sup>222</sup>Rn activities in a subset of Hyalite Canyon sites by elevation. Four samples were collected per site (open symbols), and means average results for these four collections (filled symbols). Error bars indicate one standard deviation. Site identification numbers are placed near means, and indicate the location (Fig. 1) and influencing lithology (Table 1) of samples. Site HY7 is the location most immediately below Hyalite Reservoir (Fig. 1).

Tertiary (Eocene) Absaroka volcanic rocks similar to those present in Hyalite Canyon (Smedes and Prostka, 1972) are dominated by mafic to intermediate compositions with relatively low Rb/Sr and measured <sup>87</sup>Sr/<sup>86</sup>Sr values ranging from 0.70433 to 0.70826 (Hiza, 1999; Feeley and Cosca, 2003; Lindsay and Feeley, 2003). Values for <sup>87</sup>Sr/<sup>86</sup>Sr ranging from 0.7072 to 0.7078 were reported for Eocene Absaroka volcanics east of the Hyalite area (Hiza 1999). Waters draining Eoceanaged Absaroka Volcanics in the nearby Clark's Fork of the Yellowstone drainage have <sup>87</sup>Sr/<sup>86</sup>Sr values in the range of ~0.704 to 0.705 (Horton et al. 1999; more precise values not provided).

Older Paleozoic aged carbonate sedimentary rocks in the greater Yellowstone National Park region have a higher average  $^{87}\mathrm{Sr}/^{86}\mathrm{Sr}$  value of 0.71062 (Kharaka et al., 1991). Moore-Nall (2016) reported an average  $^{87}\mathrm{Sr}/^{86}\mathrm{Sr}$  value of 0.708834 for Madison Group limestones in the Pryor Mountains  $\sim\!300$  km east of the Gallatin Range, and Frost and Toner (2004) reported a range of 0.70873 to 0.70926 for  $^{87}\mathrm{Sr}/^{86}\mathrm{Sr}$  values in Madison rocks and waters in the Big Horn Basin of Wyoming.

In contrast, much older Archean granites and gneisses, including those in the neighboring Beartooth Mountains, exhibit variable and substantially higher present-day  $^{87}\text{Sr}/^{86}\text{Sr}$  values, reflecting highly variable Rb/Sr ratios within mineral phases comprising the rock, and long time periods of  $^{87}\text{Sr}$  ingrowth. Measured  $^{87}\text{Sr}/^{86}\text{Sr}$  values for a variety of Archean-age rock types (n = 84) from the eastern and southern Beartooth Mountains had a median value of 0.76177 (Montgomery and Lytwyn, 1984; Wooden and Mueller, 1988). Water draining Precambrian granitic gneiss in the Clark's Fork basin yielded approximate  $^{87}\text{Sr}/^{86}\text{Sr}$  values of  $\sim$ 0.721 to 0.732 (Horton et al., 1999).

Although rock analysis was not undertaken as part of this study, published data corroborate assumptions made about the \$^8Sr/^86Sr compositions in primary rock types present in Hyalite Canyon (Table 2), acknowledging that differential mineral weatherability may explain some differences in waters as compared to source rocks. For expected [\$^{234}U/^{238}U] values, there are less published data. However, unaltered Eocene to Archean age rocks are all assumed to have [\$^{234}U/^{238}U] values close to secular equilibrium (equal to 1.00) regardless of lithology, although readily soluble secondary phases within soils in the region may have somewhat higher values (typically less than about 1.6) (Sharp et al., 2003). Groundwaters will have more elevated [\$^{234}U/^{238}U] values depending on aquifer character and substrate weatherability (Bourdon et al., 2003). Thus the range of [\$^{234}U/^{238}U] values observed (1.506–5.285) can be interpreted as a range of transport conditions and substrate interactions.

### 4.2. Origins of headwater compositions

Streamflow generated from groundwater in the headwaters of Hyalite and Emerald Creeks is derived primarily through water–rock interaction with Eocene volcanic rocks. Accordingly, Sr and U concentrations, Ca/Sr ratio, and alkalinity were low in higher elevation waters draining the Absaroka volcanics, likely due to igneous rocks that are less calcareous and more resistant to weathering, as well as lower temperatures that are less conducive to chemical alteration.

Values of  $^{87}$ Sr/ $^{86}$ Sr in water draining Tertiary volcanic rocks in the upper reaches of Hyalite Creek (sites HY1 and HY2) are somewhat higher than values reported for whole rock digestions in the literature. This is likely a consequence of volcanic rocks in the Gallatin Range being part of the older Washburn Group (Smedes and Prostka, 1972), which tend to have higher  $^{87}$ Sr/ $^{86}$ Sr values (median of 0.70725, Lindsay and Feely, 2003; 0.7072–0.7078, Hiza, 1999) than younger rocks in the Absaroka Supergroup. Moreover, magmas associated with early eruptions in the volcanic field may have assimilated crustal components with elevated  $^{87}$ Sr/ $^{86}$ Sr values before chambers and conduits become well established. In addition, leaching of rock and soil by water will preferentially extract Sr from the most weatherable minerals, which are not likely to have remained in equilibrium with the bulk rock over the  $\sim$ 50 million years since formation. Water may preferentially leach phases

with elevated Rb/Sr resulting in groundwater or runoff with higher  $^{87}\text{Sr}/^{86}\text{Sr}$  values. Regardless of cause, the similarity of  $^{87}\text{Sr}/^{86}\text{Sr}$  values for streamflow samples draining two separate volcanic-rock headwater basins (upper Hyalite Creek, HY1, and Emerald Creek, HY2; Fig. 1) suggest that stream flow draining subwatersheds dominated by Absaroka bedrock is well characterized with a mean value of 0.70889 in the Hyalite Creek watershed ( $\pm 0.00008~2\times$  standard deviation [SD] for n = 7 excluding 1 outlier). Lower [ $^{234}\text{U}/^{238}\text{U}$ ] values in the steeper subwatersheds in upper Hyalite Creek (HY1) and in the Emerald Creek tributary (HY2), suggest more aggressive weathering of U from soils during recharge or relatively rapid communication of meteoric water to the stream (Fig. 5).

# 4.3. Baseflow contributions from tributaries and aquifers draining sedimentary rocks

Concentrations of Sr and U, Ca/Sr ratio, and alkalinity generally increased in the middle elevations of Hyalite Creek (above 1800 m), consistent with baseflow contributions from relatively solute-rich groundwater in sedimentary bedrock units that drain to Hyalite Creek via tributaries or subsurface flow (Fig. 3). Relative to baseflow derived from Absaroka volcanics, tributaries draining aquifers in more weatherable limestones and shales are likely to contribute ion loads to the main stem that are disproportionate to their contribution to flow (Horton et al., 1999; Jacobson et al., 2002, 2003). More specifically, tributaries draining aquifers in sedimentary bedrock are more likely to contain secondary carbonates or other Ca-rich secondary phases with elevated Ca/Sr values. Consequently, inputs to streamflow along the intermediate elevations of the valley appear to be relatively minor compared to upstream flow generation, but likely contribute substantial ion loading to Hyalite Creek.

The middle reaches of Hyalite Creek drain an area dominated by Mesozoic and Paleozoic sedimentary rocks. Main stem samples (sites HY7, HY9, HY10 and HY11) show a distinct decrease in  $^{87}$ Sr/ $^{86}$ Sr values (mean value of  $0.70862 \pm 0.00013$ ,  $2 \times$  SD for n=7) interpreted to reflect addition of Sr from marine sources. Streamflow from Lick Creek draining mostly Mesozoic clastic sediments (HY3) and groundwater discharging from the Madison aquifer (sites HY16 and HY17) have lower  $^{87}$ Sr/ $^{86}$ Sr values (mean  $^{87}$ Sr/ $^{86}$ Sr values of 0.70849 and 0.70835, respectively) than those in main stem flow at the same elevation (Fig. 4). This relation is consistent with addition of Sr from marine sources, which had primary  $^{87}$ Sr/ $^{86}$ Sr between 0.7068 and 0.7082 through most of the Mesozoic and Paleozoic Eras (McArthur et al., 2001). In contrast, tributary streamflow draining a small subwatershed of volcanic rock in this reach ('Meadow' Creek; site HY13) has a higher  $^{87}$ Sr/ $^{86}$ Sr value of 0.70893, similar to values draining volcanic rocks in headwater areas.

Contributions to Hyalite Creek from aquifers in Madison Group limestones are evident from the notable increases in  $[^{234}\mathrm{U}/^{238}\mathrm{U}]$  values at intermediate elevations (Fig. 5). Springs issuing from the Madison Group limestones (HY16 and HY17) have elevated  $[^{234}\text{U}/^{238}\text{U}]$  values consistent with water that has had more extensive contact time with matrix materials, thus allowing greater incorporation of recoil <sup>234</sup>U from aquifer-rock surfaces. The large changes in  $[^{234}\text{U}/^{238}\text{U}]$  values observed in main stem samples from sites HY10 and HY11 are coupled with only small changes in U concentration and discharge, consistent with inflows having similar U concentrations but substantial enrichment in <sup>234</sup>U. Elevated  $[^{234}\text{U}/^{238}\text{U}]$  values are present in main stem samples well downstream from the contact with the Madison Group limestones, suggesting the possibility of continued influx from related karst aquifers, or reflecting the conservative nature of uranyl complexes in the dissolved load. Decreasing values of <sup>87</sup>Sr/<sup>86</sup>Sr in main stem samples below Hyalite Reservoir through this reach may be derived as a consequence of either tributary additions or gains from aquifer discharge. However, the large increase in [234U/238U] values is interpreted to be diagnostic of groundwater influxes from laterally continuous aquifers, such as those developed in Madison Group limestones. Equally elevated [<sup>234</sup>U/<sup>238</sup>U]

values are not observed in surface flow from tributaries in the same reach (sites HY13, HY12, and HY8), although values are higher than those in tributary flow above the Madison outcrop (HY3) and may indicate a contribution from Madison Group limestone aquifers or other geochemically mature groundwater as well. In support of the influence of diverse groundwaters in both upper and middle elevation inflows, <sup>222</sup>Rn concentrations were consistently elevated in upper Hyalite (HY1) as well as Lick and Moser tributaries (HY3, HY8) below the Madison inflows (Fig. 8), indicating influence of geochemically distinct and possibly younger inflows that were not discernable with U and Sr tracers.

Based on U and Sr isotope results, mixing models suggest that approximately 4% of water in Hyalite Creek at HY10 (95% confidence of 0.3% to 8.7%) can be attributed to groundwater from the Madison Group limestones entering via the subsurface somewhere below site HY7 (between elevations of 1962 m and 1909 m, Fig. 7a) (Ewing et al., 2020). While the generation of baseflow from aquifers in the Madison Group limestones is modest in Hyalite Creek relative to upstream contributions, values of  $[^{234}\text{U}/^{238}\text{U}]$  provide a sensitive indicator of the influence of storage in this important regional limestone aquifer. Although snowpack was particularly low in February 2017 (71% of average based on the Lick Creek SNOTEL), broader evaluation of the inflow rate requires knowing how prior years influenced recharge of this aquifer.

### 4.4. Contribution from Archean gneiss fracture flow

Baseflow generation from groundwater influenced by Archean gneiss is evident from progressive increases in  $^{87}$ Sr/ $^{86}$ Sr values and decreases in  $[^{234}$ U/ $^{238}$ U] values with distance downstream in the lower elevations of Hyalite Canyon. These isotopic changes are consistent with downstream evolution of main stem water towards an endmember defined by wells completed in the Archean gneiss bedrock (GW2 and GW3).

Isotopic compositions near the canyon outlet (HY5 and HY6) show differences between August and February that can be explained by seasonal differences in flow, whereby the same volume of inflow has a greater influence during lower flow in February. Substantially higher <sup>87</sup>Sr/<sup>86</sup>Sr values in February relative to August (Fig. 4, Table 3) suggest that contributions from gneiss were proportionally greater during winter than during summer, to a degree that is consistent with changes in flow. Values of [<sup>234</sup>U/<sup>238</sup>U] also show systematic differences between February and August samples (Fig. 5) that are consistent with greater contributions from sources with shorter flow paths or more intensive weathering of source rock in winter. This could reflect changes in the gneiss-derived inflow or influence of inflows from a distinct lithologic

Based on longitudinal patterns in isotopic composition, the largest influxes of water from gneiss sources appear to occur downstream from site HY15 (at elevations between 1729 and 1707, Fig. 4). A shear zone traversing the valley just below 1729 m (May, 1985) may represent a region of preferential groundwater flow. If baseflow gains are derived from groundwater discharging from fractured gneiss, [<sup>234</sup>U/<sup>238</sup>U] values suggest a very different type of water/rock interaction compared to flow in aquifers hosted by Madison Group limestones. Low [<sup>234</sup>U/<sup>238</sup>U] values imply relatively short-range connectivity such that preferential incorporation of recoil <sup>234</sup>U generated along fracture surfaces is not sufficient to increase [<sup>234</sup>U/<sup>238</sup>U] values beyond those expected after infiltration through soils.

Despite assuming a large uncertainty for the gneiss end member in mixing models of the lower end of the canyon, the Monte Carlo realizations of the mixing models and inferred mixing fractions failed to capture the compositions measured in lower Hyalite Creek mixtures (HY5, HY6; Fig. 7 b and c). The conflicting information from Sr and U data has two possible explanations. First, compositions in well-water samples may not accurately reflect the gneiss end member, which might have lower [ $^{234}$ U/ $^{238}$ U] values and U concentrations that are seasonally variable. Second, inflows from an end member not included

in the model may be affecting Hyalite Creek.

Following the first possible explanation, the shifting character of apparent inflows in lower Hyalite Canyon in February relative to August could reflect changing flow regimes through the fractured gneiss (Fig. 6). Periods of winter snowmelt on hillslopes above the lower elevations of Hyalite Creek may enhance translatory flow that alters pathways of stream flow generation from Archean gneiss bedrock at lower elevations. Similar seasonal differences in local streamflow gains were not observed at other sampling sites, suggesting this process may be limited to lower elevations with greater relative inputs of water during winter melt periods.

Alternatively, if seasonal variation reflects inflows from a distinct end member, this end member would need to have a lower <sup>87</sup>Sr/<sup>86</sup>Sr and [<sup>234</sup>U/<sup>238</sup>U] composition, somewhat similar to volcanic rocks found in the upper reaches of Hyalite Creek. Return of water derived from such rock units could be delivered by water movement through glacial till throughout the middle reaches of Hyalite Canyon, but this explanation appears physically unlikely given that return flow from the glacial till would likely be contributing to Hyalite Creek well upstream (Fig. 1). Alternately, runoff over volcanic colluvium originating from ridge tops in the lower canyon may influence geochemical composition, and this contribution would likely be small. We also note that higher U concentrations and intermediate 87Sr/86Sr composition in lower canyon samples collected in February are reasonably consistent with contributions from sedimentary tributaries in the middle canyon (Figs. 3, 4, 6), and these sedimentary units are exposed at lower elevations in the next major canyon to the west (South Cottonwood). Thus, we conclude that an additional contribution from water influenced by contact with distinct rock units, likely associated with transient runoff dynamics, cannot be ruled out as a plausible additional endmember in lower Hyalite canvon.

Despite the intriguing uncertainty about the specific character of Archean waters directly contributing to lower Hyalite, our data as a whole support the notion that is this setting,  $^{87}\mathrm{Sr}/^{86}\mathrm{Sr}$  values offer the more sensitive indicator of Archean gneiss influence. Accordingly, our data document persistent and steady inflows from the Archean gneiss during baseflow conditions in August and February 2017. Regardless of mixing model uncertainties,  $[^{234}\mathrm{U}/^{238}\mathrm{U}]$  and  $^{87}\mathrm{Sr}/^{86}\mathrm{Sr}$  data were critical to detection of baseflow contributions from different weathering components present in lower elevations of the watershed, because solute concentrations and Ca/Sr ratios were unable to identify inflow from a unique end member. Measures of  $^{222}\mathrm{Rn}$  in the lower canyon (HY5, HY6) support interpretations of groundwater inflows, though measured concentrations (~10 pCi L-1) are somewhat lower than in the middle elevation tributaries.

### 5. Conclusions

This study shows that longitudinal surveys of natural geochemical tracers and their isotopic composition can provide valuable information about groundwater sources, storage potential, and baseflow generation along stream valleys. We used <sup>87</sup>Sr/<sup>86</sup>Sr and [<sup>234</sup>U/<sup>238</sup>U] values as sensitive indicators of distinct groundwater inflows in a lithologically diverse catchment. Longitudinal <sup>222</sup>Rn assays corroborate more extensive and likely younger groundwater inflows. Radiogenic Sr and U isotopic ratios were critical to identifying and quantifying contributions from older baseflow generation that would otherwise have been invisible based on elemental concentrations alone. Moreover, longitudinal sampling allows a spatially explicit perspective on where groundwater sources occur in the catchment that would likely have been overlooked if assessed at coarser scales or only at the watershed outlet. Longitudinal sampling also allowed application of both general and localized mixing models that used combinations of tracer concentrations and isotope ratios to quantify the fractional contributions from groundwater sources. Using these models, we estimate that groundwater contribution from the Madison aquifers represents about 4% of streamflow in the

middle reaches of Hyalite Creek, and that groundwater discharging from fractured Archean gneiss supplies  ${\sim}2\%$  of local streamflow during the August baseflow period and  ${\sim}8\%$  of local streamflow during the February baseflow period. These inflows are a subset of total groundwater contributions that are evident in  $^{222}\text{Rn}$  measures, reflecting likely diversity of apparent age.

This research elucidates groundwater contributions to streamflow along Hyalite Canyon, an important water resource for agricultural and metropolitan uses in the Gallatin Valley, and analogously in intermountain basins of the region. Urban areas in intermountain basins are expanding at the same time that snowpack storage is predicated to decrease due to changes in climate patterns. Our results provide a perspective on baseflow generation along Hyalite Creek that likely represents the delayed contribution of higher elevation snowpack over interannual to decadal time scales. This work sheds light on the nature of aquifer-specific contributions to baseflow in a mountain headwater stream that provides municipal, agricultural, and ecological water supply, similar to many mountain water supplies across the intermountain west. This observation merits further study if the long-term effects of changing snowpack dynamics are to be reliably predicted.

### **Declaration of Competing Interest**

The authors declare that they have no known competing financial interests or personal relationships that could have appeared to influence the work reported in this paper.

### Acknowledgements

We thank funders including the United States Geologic Survey (USGS) National Institute of Water Resources Competitive Grants Program (#G16AP00193), the Nielsen Fellowship from the Department of Land Resources and Environmental Sciences at MSU (LRES), the Montana Agricultural Experiment Station (MAES Project Numbers MONB00389 and MONB00349), the Consortium for Research on Environmental Water Systems (NSF EPSCoR Cooperative Agreement OIA-1757351), and the Montana Water Center. We are grateful to Dale White and the US Forest Service, Custer-Gallatin National Forest for permission to sample waters in Hyalite Canyon. We also thank Erika Sturn, whose Master's work laid the groundwork for this project. We are grateful for field assistance from Ethan Wologo, Joe Capella and Simon Fordyce; and for laboratory analysis at the Montana Bureau of Mines and Geology (MBMG) by Jackie Timmer and Ashley Huft, and at the LRES Environmental Analytical Laboratory by Dr. Jane Klassen and Dr. Christine Gobrogge. Home well access was kindly provided by Cliff and Joan Montagne, and Otto and Mary Stein. Discussion of this work with Dr. Payton Gardner contributed to insight about the nature of "conservative" tracers, and we thank Dr. Gardner for his support in making <sup>222</sup>Rn measurements. We thank Rob Striegl for early support of this proposed work, and Greg Pederson for helpful review of the draft manuscript. We are grateful to Venice Bayrd for assistance with data archiving through Hydroshare. Any use of trade, firm, or product names is for descriptive purposes only and does not imply endorsement by the U.S. Government.

### Statement of data availability

Datasets, code and supplementary text are available as a data package in Hydroshare (Ewing et al., 2020).

#### References

- Amundson, R., Heimsath, A., Owen, J., Yoo, K., Dietrich, W.E., 2015. Hillslope soils and vegetation. Geomorphology 234, 122–132.
- Arendt, C.A., Aciego, S.M., Hetland, E.A., 2015. An open source Bayesian Monte Carlo isotope mixing model with applications in Earth surface processes. Geochemistry, Geophys. Geosystems 16, 1274–1292.

- Barbieri, M., Boschetti, T., Petitta, M., Tallini, M., 2005. Stable isotope (2H, 18O and 875r/86Sr) and hydrochemistry monitoring for groundwater hydrodynamics analysis in a karst aquifer (Gran Sasso, Central Italy). Appl. Geochemistry 20, 2063–2081.
- Berg, R.B., Lonn, J. D., Locke, W.W. (1999) Geologic Map of the Gardiner 30' by 60' Quadrangle, South- Central Montana.
- Berg, R.B., Lopez, D.A., Lonn, J.D. (2000) Geologic Map of the Livingston 30' x 60' Quadrangle South-Central Montana.
- Bourdon, B., Turner, S., Henderson, G.M., Lundstrom, C.C., 2003. Introduction to Useries geochemistry. Uranium-Series Geochemistry 52, 1–21.
- Bullen, T.D., White, A., Blum, A., Harden, J., Schulz, M., 1997. Chemical weathering of soil chronosequence on granitoid alluviun: II. Mineralogic and isotopic constraints on the behaviour os strontium. Geochim. Chosmo chim. Acta 60, 1807–1821.
- Capell, R., Tetzlaff, D., Malcolm, I.A., Hartley, A.J., Soulsby, C. (2011) Using hydrochemical tracers to conceptualise hydrological function in a larger scale catchment draining contrasting geologic provinces. J. Hydrol. 408, 164–177. Available at: http://dx.doi.org/10.1016/ji.jhydrol.2011.07.034.
- Capo, R.C., Chadwick, O.A., 1999. Sources of strontium and calcium in desert soil and calcrete. Earth Planet. Sci. Lett. 170, 61–72.
- Capo, R.C., Stewart, B.W., Chadwick, O.A., 1998. Strontium isotopes as tracers of ecosystem processes: Theory and methods processes: theory and methods. Geoderma 82, 197–225.
- Chabaux, F., Riotte, J., Dequincey, O., 2003. U-Th-Ra fractionation during weathering and river transport. Uranium-Series Geochemistry 52, 533–576.
- Chadwick, O.A., Derry, L.A., Bern, C.R., Vitousek, P.M., 2009. Changing sources of strontium to soils and ecosystems across the Hawaiian Islands. Chem. Geol. 267, 64–76.
- Cheng, H., Lawrence, E.R., Shen, C.C., Polyak, V.J., Asmerom, Y., Woodhead, J., Hellstrom, J., Wang, Y., Kong, X., Spötl, C., Wang, X., Calvin, A.E., 2013. Improvements in 230Th dating, 230Th and 234U half-life values, and U-Th isotopic measurements by multi-collector inductively coupled plasma mass spectrometry. Earth Planet. Sci. Lett. 371–372, 82–91.
- Covino, T.P., McGlynn, B.L., 2007. Stream gains and losses across a mountain-to-valley transition: Impacts on watershed hydrology and stream water chemistry. Water Resour. Res. 43, 1–14.
- DePaolo D. J., Lee V. E., Christensen J. N. and Maher K. (2012) Uranium comminution ages: Sediment transport and deposition time scales. Comptes Rendus Geosci. 344, 678–687. Available at: http://linkinghub.elsevier.com/retrieve/pii/S1631071312001952 [Accessed April 2, 2014].
- DePaolo, D.J., Maher, K., Christensen, J.N., McManus, J., 2006. Sediment transport time measured with U-series isotopes: Results from ODP North Atlantic drift site 984. Earth Planet. Sci. Lett. 248, 394–410.
- Dixon, J.L., Chadwick, O.A., Vitousek, P.M., 2016. Climate-driven thresholds for chemical weathering in postglacial soils of New Zealand. J. Geophys. Res. Earth Surf. 121. 1619–1634.
- DNRC M. (2014) Middle Creek Dam (Hyalite) Fact Sheet.
- Dosseto, A., Bourdon, B., Turner, S.P., 2008. Uranium-series isotopes in river materials: Insights into the timescales of erosion and sediment transport. Earth Planet. Sci. Lett. 265, 1–17.
- Dosseto A., Buss H. L. and Chabaux F. (2014) Age and weathering rate of sediments in small catchments: The role of hillslope erosion. Geochim. Cosmochim. Acta 132, 238–258. Available at: http://linkinghub.elsevier.com/retrieve/pii/S0016703714000982 [Accessed July 11, 2014].
- Drexler J. Z., Paces J. B., Alpers C. N., Windham-Myers L., Neymark L. A., Bullen T. D. and Taylor H. E. (2014) 234U/238U and d87Sr in peat as tracers of paleosalinity in the Sacramento-San Joaquin Delta of California, USA. Appl. Geochemistry 40, 164–179. Available at: http://dx.doi.org/10.1016/j.apgeochem.2013.10.011.
- Emanuel, R.E., Hazen, A.G., Mcglynn, B.L., Jencso, K.G., 2014. Vegetation and topographic influences on the connectivity of shallow groundwater between hillslopes and streams. Ecohydrology 7, 887–895.
- Ewing, S.A., Miller, F.R., Payn, R.A., Paces, J.B., 2020. Radon, uranium, strontium and other compositional analytical data documenting groundwater contributions along a mountain headwater catchment in Hyalite Canyon, MT, USA (2016-2018). Hydroshare, Available at: https://doi.org/10.4211/hs.46a2ec0b25ba406bbf8571d
- Ewing, S.A., Paces, J.B., O'Donnell, J.A., Jorgenson, M.T., Kanevskiy, M.Z., Aiken, G.R., Shur, Y., Harden, J.W., Striegl, R., 2015. Uranium isotopes and dissolved organic carbon in loess permafrost: Modeling the age of ancient ice. Geochim. Cosmochim. Acta 152, 143–165.
- Faure, G., Mensing, T.M., 2004. Isotopes: Principles and Applications, 3rd ed. John Wiley & Sons Inc, Hoboken, NJ, New Jersey.
- Faure, G., Mensing, T.M., 2005. Isotopes Principles and Applications, 3rd Edition. John Wiley & Sons, Hoboken, New Jersey.
- Feeley, T.C., Cosca, M.A., 2003. Time vs. composition trends of magmatism at Sunlight volcano, Absaroka volcanic province, Wyoming. Geol. Soc. Am. Bull, 714–728.
- Frost, C.D., Toner, R.N., 2004. Strontium isotopic identification of Water-Rock Interaction and Ground Water Mixing. Ground Water 42, 418–432.
- Gardner, W.P., Harrington, G.A., Solomon, D.K., Cook, P.G., 2011. Using terrigenic 4He to identify and quantify regional groundwater discharge to streams. Water Resour. Res. 47, 1–13.
- Gedeon J. (2015) Tourist traffic skyrockets in popular Bozeman recreation area. NBC Mont
- Hart, W.S., Quade, J., Madsen, D.B., Kaufman, D.S., Oviatt, C.G., 2004. The 87Sr/86Sr ratios of lacustrine carbonates and lake-level history of the Bonneville paleolake system. Bull. Geol. Soc. Am. 116, 1107–1119.

- Hinckley, E.L.S., Ebel, B.A., Barnes, R.T., Anderson, R.S., Williams, M.W., Anderson, S.P., 2014. Aspect control of water movement on hillslopes near the rain-snow transition of the Colorado Front Range. Hydrol. Process. 28, 74–85.
- Hiza, M.M., 1999. The geochemistry and geochronology of the Eocene Absaroka volcanic province, northern Wyoming and southwest Montana. Thesis, Oregon State University, USA.
- Hoehn, E., Stauffer, F., Dracoss, T., 1992. Radon-222 as a Groundwater Tracer. A Laboratory Study. 26, 734–738.
- Hogan, J.F., Blum, J.D., 2003. Tracing hydrologic flow paths in a small forested watershed using variations in 87 Sr/ 86 Sr, [Ca]/[Sr], [Ba]/[Sr] and δ 18 O. Available at: Water Resour. Res. 39, 1282 http://www.agu.org/pubs/crossref/2003/ 2002WR001856.shtml.
- Horton, T.W., Chamberlain, C.P., Fantle, M., Blum, J.D., 1999. Chemical weathering and lithologic controls of water chemistry in a high-elevation river system: Clark's Fork of the Yellowstone river. Wyoming and Montana. Water Resour. Res. 35, 1643–1655.
- Hoylman, Z.H., Jencso, K.G., Hu, J., Martin, J.T., Holden, Z.A., Seielstad, C.A., Rowell, E. M., 2018. Hillslope Topography Mediates Spatial Patterns of Ecosystem Sensitivity to Climate. J. Geophys. Res. Biogeosciences 123, 353–371.
- Jacobson, A.D., Blum, J.D., Chamberlain, C.P., Craw, D., Koons, P.O., 2003. Climatic and etctonic controls on chemical weathering in the New Zealand Southern Alps. Geochim. Cosmochim. Acta 67, 29–46.
- Jacobson, A.D., Blum, J.D., Walter, L.M., 2002. Reconciling the elemental and Sr isotope composition of Himalayan weathering fluxes: Insights from the carbonate geochemistry of stream waters. Geochim. Cosmochim. Acta 66, 3417–3429.
- Jaffey, A.H., Flynn, K.F., Glendenin, L.E., Bentley, W.C., Essling, A.M., 1971. Precision measurement of half-lives and specific activities of U235 and U238. Phys. Rev. C 4, 1889–1906.
- Jasechko, S., 2016. Partitioning young and old groundwater with geochemical tracers. Chem. Geol. 427, 35-42.
- Jasechko, S., Kirchner, J.W., 2016. Substantial proportion of global streamflow less than three months old. Nat, Geosci.
- Jencso, K.G., McGlynn, B.L., 2011. Hierarchical controls on runoff generation: Topographically driven hydrologic connectivity, geology, and vegetation. Water Resour. Res. 47.
- Jencso, K.G., McGlynn, B.L., Gooseff, M.N., Wondzell, S.M., Bencala, K.E., Marshall, L.A., 2009. Hydrologic connectivity between landscapes and streams: Transferring reachand plot-scale understanding to the catchment scale. Water Resour. Res. 45.
- Kellogg, K.S., Williams, V.S., 2006. Geologic Map of the Ennis 30' by 60' Quadrangle Madison and Gallatin Counties. Montana, Park County, Wyoming.
- Kharaka Y. K., Mariner R. H., Bulled R. D., Kennedy B. M. and Sturchio N. C. (1991) Geochemical Investigations of Hydraulic connections between the Corwin Springs Know Geothermal Resources Area and Adjacent Parts of Yellowstone National Park, in Sorrey, M.L., Effects of potential geothermal development in the Corwin Springs Known Geother.
- Kirk, K.B., 2002. A preliminary investigation of the Madison aquifer for a drinking water supply in Bozeman. Thesis, Montana State University, Montana Abstract.
- Knowles, N., Park, M., Dettinger, M.D., 2005. Trends in Snowfall versus Rainfall in the Western United States Trends in Snowfall versus Rainfall in the Western United States. J. Clim. 19, 4545–4559.
- Kramer, C., 2013. A History of Bozeman's Water System Part III. Bozeman Mag. Lindsay, C.R., Feeley, T.C., 2003. Magmagenesis at the Eocene Electric Peak Sepulcher Mountain complex, Absaroka Volcanic Province. USA 67, 53–76.
- Ludwig, K.R., Wallace, A.R., Simmons, K.R., 1985. The Schwartzwalder uranium deposit, II: Age of uranium mineralization and lead isotope constraints on genesis. Econ. Geol. 80, 1858–1871.
- Maher, K., DePaolo, D.J., Christensen, J.N., 2006. U-Sr isotopic speedometer: Fluid flow and chemical weathering rates in aquifers. Geochim. Cosmochim. Acta 70, 4417–4435
- May, K.A., 1985. Archean geology of a part of the northern Gallatin Range, southwest Montana. Montana State University, Thesis.
- McArthur, J.M., Howarth, R.J., Bailey, T.R., 2001. Strontium Isotope Stratigraphy: LOWESS Version 3: Best Fit to the Marine Sr-Isotope Curve for 0–509 Ma and Accompanying Look-up Table for Deriving Numerical Age. J. Geol. 109, 155–170.
- McArthur, J.M., Rio, D., Massari, F., Castradori, D., Bailey, T.R., Thirlwall, M., Houghton, S., 2006. A revised Pliocene record for marine-87Sr/86Sr used to date an interglacial event recorded in the Cockburn Island Formation, Antarctic Peninsula. Palaeogeogr. Palaeoclimatol. Palaeoecol. 242, 126–136.
- McGlynn, B.L., McDonnell, J.J., 2003. Quantifying the relative contributions of riparian and hillslope zones to catchment runoff. *Water Resour*. Res. 39.
- McGuire, K.J., McDonnell, J.J., Weiler, M., Kendall, C., McGlynn, B.L., Welker, J.M., Seibert, J., 2005. The role of topography on catchment-scale water residence time. Water Resour. Res. 41, 1–14.
- Montgomery, C.W., Lytwyn, J.N., 1984. Rb-Sr Systematics and Ages of Principal Precambrian Lithologies in the South Snowy Block, Beartooth Mountains. J. Geol. 92, 103–112.
- Montgomery, D.R., 1999. Process domains and the river continuum. J. Am. Water Resour. Assoc. 35, 397–410.
- Moore-Nall, A.L. (2016) Structural controls and chemical characterization of brecciation and uranium vanadium mineralization in the Northern Bighorn Basin. ProQuest Diss. Theses, 376. Available at: http://proxy.library.vcu.edu/login?url=https://search.pr

- $oquest.com/docview/1877615298?accountid=14780\%0Ahttp://vcu-alma-primo. hosted.exlibrisgroup.com/openurl/VCU/vcu_services_page?url_ver=Z39.88-2004\&rft_val_fmt=info:ofi/fmt:kev:mtx:dissertation&genre=diss.$
- Négrel, P., Petelet-giraud, E., Widory, D., 2004. Strontium isotope geochemistry of alluvial groundwater: a tracer for groundwater resources characterisation. Hydrol. Earth Syst. Sci. 8, 959–972.
- Paces, J.B., Long, A.J., Koth, K., 2015. Potential Application of Radiogenic Isotopes and Geophysical Methods to Understand the Hydrothermal System of the Upper Geyser Basin. Yellowstone National Park.
- Paces, J.B., Wurster, F.C., 2014. Natural uranium and strontium isotope tracers of water sources and surface water-groundwater interactions in arid wetlands - Pahranagat Valley, Nevada. USA. J. Hydrol. 517, 213–225.
- Payn, R.A., Gooseff, M.N., McGlynn, B.L., Bencala, K.E., Wondzell, S.M., 2009. Channel water balance and exchange with subsurface flow along a mountain headwater stream in Montana, United States. Water Resour. Res. 45.
- Payn, R.A., Gooseff, M.N., McGlynn, B.L., Bencala, K.E., Wondzell, S.M., 2012. Exploring changes in the spatial distribution of stream baseflow generation during a seasonal recession. Water Resour. Res. 48, 1–15.
- Pierret, M.C., Stille, P., Prunier, J., Viville, D., Chabaux, F., 2014. Chemical and U-Sr isotopic variations in stream and source waters of the Strengbach watershed (Vosges mountains, France). Hydrol. Earth Syst. Sci. 18, 3969–3985.
- Roback, R.C., Johnson, T.M., Mcling, T.L., Murrell, M.T., Luo, S., Ku, T., 2001. Uranium isotopic evidence for groundwater chemical evolution and flow patterns in the eastern Snake River Plain aquifer, Idaho. Geol. Soc. Am. Bull. 113, 1133–1141.
- Ryu, J., Lee, K., Chang, H., Cheong, C., 2009. Uranium isotopes as a tracer of sources of dissolved solutes in the Han River, South Korea. Chem. Geol. 258, 354–361.
- Schubert M., Buerkin W., Peña P., Lopez A. E. and Balcázar M. (2006) On-site determination of the radon concentration in water samples: Methodical background and results from laboratory studies and a field-scale test. 41, 492–497.
- Sharp W. D., Ludwig K. R., Chadwick O. A., Amundson R. and Glaser L. L. (2003) Dating fluvial terraces by 230Th/U on pedogenic carbonate, Wind River Basin, Wyoming. Quat. Res. 59, 139–150. Available at: http://linkinghub.elsevier.com/retrieve/pii/S0033589403000036 [Accessed October 4, 2014].
- Silverman, N.L., Maneta, M.P., 2016. Detectability of change in winter precipitation within mountain landscapes: Spatial patterns and uncertainty. Water Resour. Res. 52, 4301–4320.
- Silverman N. L., Maneta M. P., Chen S.-H. and Harper J. T. (2013) Dynamically downscaled winter precipitation over complex terrain of the Central Rockies of Western Montana, USA. Water Resour. Res. 49, 458–470. Available at: http://doi. wiley.com/10.1029/2012WR012874 [Accessed April 3, 2014].
- Smedes, H.W., Prostka, H.J., 1972. Stratigraphic Framework of the Absaroka Volcanic Supergroup in the Yellowstone National Park Region. Geol. Surv. Prof. Pap. 729-C, 1–43.
- Soulsby, C., Tetzlaff, D., 2008. Towards simple approaches for mean residence time estimation in ungauged basins using tracers and soil distributions. J. Hydrol. 363, 60–74.
- Steiger, R.H., Jäger, E., 1977. Subcommission on geochronology: Convention on the use of decay constants in geo- and cosmochronology. Earth Planet. Sci. Lett. 36, 359–362.
- Suksi, J., Rasilainen, K., Pitkanen, P., 2006. Variations in 234U/238 U activity ratios in groundwater — A key to flow system characterisation? Phys. Chem. Earth 31, 556–571.
- United States Department of Agriculture N. R. C. S. (1996) Soil Survey of Gallatin National Forest, Montana.
- Vuke, S.M., Lonn, J.D., Berg, R.B., Schmidt, C.J., 2002. Geologic map of the bozeman 30' x 60' Quadrangle Southwestern Montana. Open-File Report 648.
- Vuke S. M., Porter K. W., Lonn J. D. and Lopez D. A. (2007) Geologic Map of Montana edition 1.0.
- Weber, M., 1965. General geology and geomorphology of the Middle Creek area, Gallatin County. Thesis, Montana State University, Montana.
- White, A.F., Schulz, M.S., Lowenstern, J.B., Vivit, D.V., Bullen, T.D., 2005. The ubiquitous nature of accessory calcite in granitoid rocks: Implications for weathering, solute evolution, and petrogenesis. Geochim. Cosmochim. Acta 69, 1455–1471.
- White, A.F., Schulz, M.S., Stonestrom, D.A., Vivit, D.V., Fitzpatrick, J., Bullen, T.D., Maher, K., Blum, A.E., 2009. Chemical weathering of a marine terrace chronosequence, Santa Cruz, California. Part II: Solute profiles, gradients and the comparisons of contemporary and long-term weathering rates. Geochim. Cosmochim. Acta 73, 2769–2803.
- Wilson, J.L., Guan, H. (2004) Mountain-Block Hydrology and Mountain Front Recharge. In Groundwater Recharge in a Desert Environment: The Southwestern United States (eds. J. F. Hogan, F. M. Phillips, and B. R. Scanlon). American Geophysical Union. pp. 113–138.
- Wooden, J.L., Mueller, P.A., 1988. Pb, Sr, and Nd isotopic compositions of a suite of Late Archean, igneous rocks, eastern Beartooth Mountains: implications for crust-mantle evolution. Earth Planet. Sci. Lett. 87, 59–72.
- Yang, J., Mcmillan, H., Zammit, C., 2017. Modelling Surface water-groundwater interaction in New Zealand: Model development and application. Hydrol. Process. 31, 1099–11085.